NASA Technical Memorandum 103786

Vapor Crystal Growth Technology Development—Application to Cadmium Telluride

Franz Rosenberger and Michael Banish
University of Alabama in Huntsville
Huntsville, Alabama

and

Walter M.B. Duval
Lewis Research Center
Cleveland, Ohio

December 1991

NASA

VAPOR CRYSTAL GROWTH TECHNOLOGY DEVELOPMENT - APPLICATION TO CADMIUM TELLURIDE

VAPOR CRYSTAL GROWTH TECHNOLOGY DEVELOPMENT

Franz Rosenberger and Michael Banish
University of Alabama in Huntsville
Center for Microgravity and Materials Research
Huntsville, Alabama 35899

and

Walter M.B. Duval
National Aeronautics and Space Administration
Lewis Research Center
Cleveland, Ohio 44135

SUMMARY

A novel technology for the growth of bulk crystals by physical vapor transport has been developed and applied to cadmium telluride. In particular, this technology makes use of effusive ampoules, in which part of the vapor contents escapes to a vacuum shroud through defined leaks during the growth process. This approach has the advantage over traditional sealed ampoule techniques that impurity vapors and excess (incongruent) vapor constituents are continuously removed from the vicinity of the growing crystal. Consequently, growth rates are obtained routinely at magnitudes that are rather difficult to achieve in closed ampoules. Other advantages of this **effusive ampoule physical vapor transport** (EAPVT) technique include (1) the predetermination of transport rates based on simple fluid dynamics and engineering considerations, and (2) the growth of the crystal from close-to-congruent vapors, which largely alleviates the compositional nonuniformities resulting from buoyancy-driven convective transport.

After concisely reviewing earlier work on improving transport rates, nucleation control, and minimization of crystal-wall interactions in vapor crystal growth, this report gives a detailed technical account of the largely computer controlled EAPVT experimentation developed in our laboratory. In addition, after a summary of the earlier work on the crystal growth of cadmium telluride, our own efforts to grow this material by EAPVT are described in detail. These efforts have resulted in largely single crystalline boules of 25 mm diameter and length, with dislocation (etch pit) densities as low as 2×10^3 cm^{-2}. Tellurium precipitates were essentially limited to grain and twin boundaries. Typical carrier concentrations were 8×10^{15} cm^{-3}. Optical absorption measurements showed close to theoretical transivities between 860 nm and 32 μm, indicating high purity of the material. Further measures for the improvement of the growth conditions for obtaining better crystal quality are suggested.

1. INTRODUCTION

Crystalline solid state devices are the mainstay of modem electronic and opto-electronic technology. Device material is largely obtained through crystallization from

melts and vapors. Crystallization from vapors has various advantages over melt growth (refs. 1 to 3). These advantages result mostly from: (1) the lower temperatures involved, (2) the lower atomic roughness and consequent growth rate anisotropy of most vapor-solid interfaces (refs. 4 and 5) which results in higher morphological (interfacial shape) stability (refs. 6 to 10) during growth, and (3) the fact that particulates and low vapor pressure impurities are readily retained in the source material.

Consequently, crystallization from vapors has gained ever increasing importance in materials preparation, in particular for the large-scale manufacture of electronically active and insulating layers. Bulk crystals, on the other hand, are not grown in large quantities from vapors, in spite of the potential for achieving higher structural quality. This is because most workers experience slow growth rates and complex transport behavior. However, as will be outlined in the following section, these difficulties are not inherent features of crystallization from vapors but are largely the consequences of traditional vapor growth technology that allows only for rather limited control of the transport and growth parameters.

For improving the design of vapor crystal growth equipment a more quantitative understanding of the dynamics of transport in vapors is needed. In the past, due to the complexity of the transport phenomena encountered (refs. 1 to 3 and 11), progress in vapor crystal growth has been mostly made through intuition and experience. In the last few years, however, theoretical and experimental work has shed considerable light on heat, mass and momentum transport in vapor transport processes involving ampoules (refs. 1 to 3, 7, and 12 to 17). Applications of this improved understanding of the transport limiting parameters, in our laboratory (refs. 14, 18, and 19) and by other workers (refs. 20, 21, and 91), have lead to drastically increased growth rates and better control of bulk vapor crystal growth. Specifically, with CdS we have obtained transport rates approaching those of melt growth (ref. 19).

Utilizing these new insights, we have developed a novel vapor growth technology with financial support by the National Aeronautics and Space Administration (Contract NAS3-25361) and the Boeing Aerospace Company (Contract HD 6763). This report summarizes this development and the application of the technology to the growth of CdTe.

1.1 CONTROL REQUIRED FOR HIGH-QUALITY VAPOR PHASE CRYSTAL GROWTH

We define here "high-quality" crystal growth as a procedure that reproducibly and within an economically feasible time, yields crystals of sufficient size that have: (1) sufficient uniformity in chemical composition, i.e., with respect to tolerable impurity or desirable dopant concentrations and/or stoichiometry of the host lattice, and (2) a structural defect concentration low and uniform enough to be readily used in a planned fundamental study or device application.

In vapor phase crystal growth the attainment of such high quality requires the following measures and control of parameters:

(1) Nucleation must be restricted to a few events at a designated location at the beginning of the crystallization process. This can be achieved by either seeding and/or careful programming of the supersaturation. Failure to control and separate nucleation and growth stages results in many small crystals. These interfere through their vapor transport fluxes, which leads to nonuniformities in growth conditions, that aggravate the nonuniformities inherently induced by the growth container (refs. 12 and 13). If the crystallites are closely spaced, additional growth leads eventually to mechanical interference that often results in structural defects.

(2) Growth must be conducted under steady-state conditions. Nonsteady transport fluxes in the bulk vapor tend to result in a nonuniform composition of the crystals; for a detailed review see chapter 6.5 in reference 22. Nonsteady transport due to instabilities in free convection can be alleviated by utilizing a microgravity environment and/or fluid dynamically more advantageous design of the thermal and momentum boundary conditions.

(3) Growth must be conducted under uniform concentration and temperature conditions across the vapor-solid interface(s). Nonuniform supply fields tend to result in nonuniformly composed crystals. Certain convection patterns can cause pronounced compositional nonuniformities in the vapor phase (ref. 13). Drastic reduction of free convection, e.g., in a microgravity environment, can lead to more uniform (diffusion-controlled) transport. It should be noted that convective vapor transport is not a priori "detrimental" to high-quality crystal growth, only nonuniform and/or time dependent nutrient supply due to convection (or other means such as inadequate temperature stability) is.

(4) Growth must be conducted such that morphological stability (refs. 6 to 10, 23 and 24) is maintained. Shape changes during growth tend to be associated with compositional variations even under steady-state and uniform supply conditions in the bulk vapor phase. The morphologically destabilizing effect of (economically desirable) higher growth rates can be counteracted if the interfacial temperature gradients can be controlled independently from the interfacial concentration gradients.

(5) Growth must be conducted such that forces acting on the crystal from the growth environment, in particular during cooldown, do not exceed the elastic limit of the lattice. For materials that are soft at the growth temperature the mere weight of a crystal may lead to its plastic deformation and associated defect formation. In such a case a microgravity environment may become essential for the achievement of high structural quality. But even rather hard materials may become severely flawed during growth and/or cooldown, when they stick to the container, unless there is a, typically impractical, close match in thermal expansion coefficients. Hence, a judicious design of the seed/crystal holding device and growth geometry is essential, with minimization of the mechanical contact area, but without loss of the cooling function of the immediate crystal environment.

(6) Appropriate purity and stoichiometry conditions must be maintained during growth. This requires a judicious choice of growth apparatus materials and configuration. Further purification during the growth process is desirable, and close control of a compound's partial pressure may be needed to define the stoichiometry (see e.g., chapter 4.4 in refs. 22 and 25). For CdTe, for instance, stoichiometry shifts or dopant concentrations of 1 ppm (1.6×10^{16} atoms/cm^3 for CdTe) are sufficient to shift the resistivity from semi-insulating to a few Ω cm (refs. 49 and 61).

1.2 EARLIER WORK ON TRANSPORT AND CONTROL IN BULK CRYSTAL GROWTH FROM VAPORS

Crystal growth by vapor transport is traditionally conducted in simple, rounded end, closed ampoules. All constituents of the transport system are loaded and sealed into a (silica) tube under ambient conditions and brought to operating conditions in some heating arrangement. The only external control then left consists in imposing a specific temperature distribution on the wall of the sealed-off ampoule.

1.2.1 Transport Rates

It is commonly experienced that a material, in order to be transported with reasonable rates by closed ampoule physical vapor transport (PVT), must have a minimum vapor pressure of the order of one tort or so at the process temperature. Crystals of lower vapor pressure materials are customarily grown by chemical vapor transport (CVT) (ref. 26).

On the other hand, based on simple gas kinetic arguments (ref. 27) one predicts that in PVT growth rates of 1 cm per day should be readily obtainable even at vapor pressures as low as 10^{-2} torr. As we have shown earlier (refs. 12 and 14), this discrepancy is mostly due to transport limitations from diffusion that is practically unavoidable in the closed ampoule approach. Impurity concentrations or deviations in the vapor stoichiometry as low as 10^{-4} mol fractions can lead to sizeable diffusion barriers via accumulation of the excess component by the sweeping net transport flux from the subliming source and the growing crystal (ref. 12). Some stoichiometry control can be gained by multiple sublimation of the starting material. Careful vacuum baking and sealing of the ampoule will reduce foreign gas adsorbed on ampoule walls and source material. However, foreign gas occluded in the source material, together with stoichiometry shifts during sublimation, make it practically impossible to maintain congruent vapor composition in closed ampoule crystal growth. Also, the usual "high-vacuum" sealing of silica ampoules can lead to significant partial pressures of impurity gases inside an ampoule (ref. 28).

Efforts to improve mass transfer in vapor transport followed two routes: (a) use of forced carrier gas flow in an open system (refs. 29 to 31); and (b) continuous removal of the barrier-forming component (together with some growth species) via effusion from

semi-closed ampoules, see references 36 to 44 in reference 14 (refs. 18 to 21 and 91 and references therein).

For this latter approach, our group has shown for the first time that upon placement of the effusion hole close to the growing crystal, transport fluxes are only limited by viscous interaction of the flow with the ampoule walls (ref. 14). Hence, we have coined this transport mode as "diffusionless transport" and the growth technique as "effusive ampoule physical vapor transport (EAPVT)." The transport rates obtained in the EAPVT of iodine (ref. 14) and CdS (ref. 19) agreed with theoretical predictions for viscous flows, which are conceptually much simpler than the complex flows encountered in closed ampoules (refs. 1 to 3, 12, 13, 15 to 17, and 32 to 35) and, hence, lend themselves more readily to design and scaling considerations.

1.2.2 Nucleation Control, Seeding and Morphological Stability

Many workers find it difficult to avoid parasitic nucleation in the part of a vapor growth ampoule that is adjacent to the main crystal; for a detailed compilation see reference 36. Linear axial temperature profiles imposed on an ampoule often lead to a jumble of crystals propagating for several centimeters from the colder ampoule end, where one attempts to grow the main crystal. This is a direct consequence of the linear temperature profile (ref. 14). With a temperature hump between source and growing crystal this unwanted nucleation can be largely alleviated, as several practitioners have demonstrated; for references and thermal measures to realize this design criterion see reference 14.

Nucleation on the ampoule wall almost always requires a higher supersaturation than growth onto an existing crystal. Hence, with the introduction of a seed (refs. 36 to 38) in combination with the appropriate temperature distribution (the temperature hump mentioned above and radiation cooling (refs. 21, 39, and 40) or forced convection cooling (ref. 18), and references in ref. 37 of the seeding area) one can more readily avoid parasitic growth in an ampoule. Various advantageous seed mounting techniques have been presented in references 18 and 36 to 39. A seed permits also the predetermination of the crystal orientation with respect to the ampoule geometry. This may be advantageous for morphological stability (e.g., facets normal to main transport flux) and mechanical interaction reasons (stiffest crystal axis parallel to support plate).

The quantitative conditions under which vapor-solid interfaces lose their morphological stability are not well understood at this point (ref. 7). Yet experience shows that the morphologically destabilizing effect of the nutrient supply field can be counteracted if the interfacial temperature gradient can be controlled independently from the interfacial concentration gradients. In a two-temperature closed-ampoule transport system there is no possibility to independently control the bulk transport flux (that governs the interfacial concentration gradient) and the interfacial concentration gradient. Some limited uncoupling between free convective flow strength and interfacial concentration conditions can be obtained by the use of a three-temperature arrangement (refs. 41 and 42). In an EAPVT system however, where due to the quasi-congruent composition of the vapor

interfacial concentration gradients are minimal, morphological instabilities are rarely encountered even at high growth rates.

1.2.3 Minimization of Crystal-Ampoule Interaction

As mentioned in section 1.1, any mechanical interaction between crystal and ampoule, in particular during cooldown, must be minimized if high structural crystal quality is desired. Optimally, the growth environment is designed such that the growing crystal does not contact the ampoule wall, except in the seed area. This can be achieved if the ampoule wall is kept somewhat warmer than the growing crystal, as has been achieved through utilization of the different optical (infrared) properties of the growing crystal, silica ampoule wall or an optically active insert (refs. 43 to 50).

1.3 STATUS OF MICROGRAVITY VAPOR PHASE CRYSTAL GROWTH ACTIVITIES

Vapor crystal growth experiments under low gravity conditions have been conducted by investigators in the U.S. (refs. 51 to 55), Europe (refs. 56 and 57), USSR (ref. 58) and are being prepared by Japanese workers (ref. 59). The U.S. efforts have produced very promising results. Wiedemeier et al. (refs. 51 to 53) have obtained significant improvements in size and morphology of GeSe, GeTe, and GeS crystals as compared to earth grown samples of the same materials. Van den Berg et al. (refs. 54 and 55) have grown HgI_2 crystals in space that were more uniform in composition than ground grown samples and showed a mobility for both holes and electrons which was more than five times higher than those found before in HgI_2. Siffert and coworkers (ref. 57) have obtained improvement in both the etch pit density and the resistivity of CdTe crystals grown from vapor on Space-Lab D-1. They concluded that this may indicate that the absence of gravity-driven convective flows, temperature, and concentration fluctuations inhibits the formation of most defects.

All low gravity vapor growth experiments conducted to date have been carried out in closed ampoules; i.e., all constituents of the system are loaded and sealed into a (silica) tube at room temperature and then brought to operating conditions in some heating arrangement. As pointed out in section 1.2, the only external control possibility then left consists in imposing a specific temperature distribution on the ampoule. Recognizing the desirability of a better control of the supersaturation at the crystal, French workers have recently developed a three-temperature arrangement for vapor crystal growth in space (refs. 41 and 42). The flux is driven by the temperature (chemical potential) difference between the outermost two temperature zones and growth occurs at some in-between temperature. Though this approach gives some added degree of control over the traditional two-zone approach, the bulk and interfacial transport conditions are still strongly coupled.

2. CADMIUM TELLURIDE

The principal uses of cadmium telluride are for optoelectronic devices, including solar cells, gamma ray detectors, infrared transmitting windows, and as substrates for the epitaxial growth of HgCdTe.

2.1 PROPERTIES IMPORTANT FOR VAPOR CRYSTAL GROWTH

The cadmium and tellurium vapor pressures above congruently subliming CdTe in the temperature range of 780 to 939 °C were measured by Brebrick and Strauss (ref. 60). They found that the vapor sublimes stoichiometrically to 1 part in 200, in this temperature range. The congruent point of cadmium telluride (the element ratio at which there is no composition change during a phase transition) lies, depending on the growth temperature, 1 to 10 ppm on the tellurium side of the exact stoichiometry point (one tellurium atom to one cadmium atom) (ref. 61 and 62). Thus, congruently grown CdTe is p-type. This small composition shift has been inferred from conductivity measurements. Direct determinations of such small stoichiometry shifts are not possible at this point. The lowest total vapor pressure in a condensed phase system occurs at the congruent point; this is often referred to as the P_{min} condition (refs. 22, 25, and 61). If a condensed compound differs from the congruent composition it will predominantly vaporize the excess component. This results in a higher total vapor pressure. Note that such incongruent vaporization of a (source) material leads in crystal growth to an accumulation of the excess component at the growing crystal. This diffusion barrier limits further transport. Therefore, for rapid vapor transport and crystal growth, one must either attain close to congruent vapor composition (P_{min} conditions) or continuously remove the excess component.

In this context it also important to remember that providing a stoichiometric vapor does not necessarily results in a stoichiometric crystal. This is particularly true for CdTe that, as depicted in Figure 1, possesses a bulbous solid-phase stability region that is rather narrow at lower temperatures (ref. 62). Hence, congruently condensing CdTe tends to form (infrared absorbing) tellurium precipitates on cooling. Note that semi-insulating material could be obtained precipitate free. To avoid the formation of precipitates, i.e., to make sure that the stoichiometry of the condensing material lies within the narrow low-temperature existence range of the compound, a Cd rich source composition is required. This can be achieved either through preannealing of the source material in a Cd overpressure, or - preferably, since better defined - through the use of a cadmium vapor reservoir at a fixed temperature. However, in a closed ampoule vapor growth technique both a source composition shift towards cadmium rich or an increase in the cadmium partial pressure would decrease the transport rates to uneconomic levels.

Cadmium telluride readily twins during crystal growth. For instance, it has been reported by one research group that of 100 crystals grown from the vapor all contained at least one twin (ref. 63). This is due to the fact that in cadmium telluride both, the stacking fault formation energy and critical resolved shear stress are very low (both 10

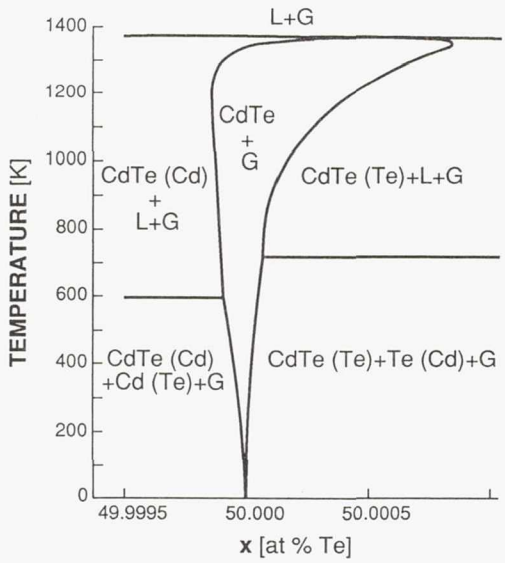

Figure 1.–Part of the T-x diagram of the Cd-Te system showing the existence region of CdTe. After [62].

times less than for Si (ref. 64)). Hence, for a minimization of the formation of dislocations, grain boundaries and twins, thermal gradients in the grown crystal should be as low as possible. Furthermore, the thermal expansion coefficient of CdTe is an order of magnitude higher than that of silica (refs. 65 and 66). Consequently, mechanical interactions between crystal and ampoules must be minimized. This is not trivial, since the native oxides of CdTe tend to adhere to uncoated silica glass that contains any significant OH^- ion concentrations (ref. 66). Thus the use of silica with low OH^- concentration and CdTe with low native oxide concentration, as well as exclusion of other oxygen sources during growth is important. Though the vapor pressure of the (pure) native oxides, CdO and TeO_2 (refs. 67 and 68), are at least an order of magnitude lower than that of CdTe, the fugacity of the native oxides in CdTe is not known. Hence, it is not clear whether sublimation in a closed vapor growth arrangement can reduce the native oxide concentrations. It has recently been shown in melt grown material that the etch pit density is proportional to the TeO_2 concentration (in the CdTe crystal), and this was correlated to the O_2 or H_2O concentration sealed into the ampoule prior to growth (ref. 69).

2.2 CURRENT STATUS OF CdTE CRYSTAL GROWTH

The majority of commercially available CdTe crystals are grown from the melt by the self-nucleated Bridgman technique with growth rates of 0.5 to 2 cm/day. The crystals are typically rapidly cooled to reduce precipitate formation. The mostly polycrystalline boules are then mined for single crystal sections. Typical etch pit densities (EPD) in commercially grown CdTe are in the high 10^4 to $10^5/cm^2$ range. N-type or semi-insulating material is mostly obtained through doping with indium, rather than through increasing the cadmium partial pressure during growth.

On a research level, significant advances in crystal quality have been made recently in growth from melts. Almost entirely twin-free single crystal boules with EPD of $1x10^4/cm^2$ where obtained by a seeded vertical gradient freeze technique (ref. 70). The lack of twinning was believed to be the result of the low radial and axial temperature gradients, which were less than 1 °C/cm and 2 to 3 °C/cm, respectively. Similar values of EPD (1 to $5x10^4/cm^2$) in twinned material were obtained by a modified vertical Bridgman technique with again low axial temperature gradients (ref. 71). Song et al. (ref. 72) showed that the conductivity can be shifted from p-type to semi-insulating and n-type with increasing partial pressure of cadmium. Lay et al. (ref. 73) and Cheuvart et al. (ref. 74) obtained crystal boules that were 75 percent single crystalline, with EPD as low as $2x10^4/cm^2$ via a horizontal Bridgman technique with a cadmium overpressure.

Though there is an extensive research literature on the vapor growth of CdTe, to date vapor phase growth of this material has not been applied on a commercial scale. Tuller et al. (ref. 75) grew crystals for laser windows by physical vapor deposition in an open tube with separate cadmium and tellurium sources using He or He plus H_2 as the carrier gas. They showed that the stoichiometry (as well as the free carrier concentration) can be controlled by adjustment of the Cd/Te ratio, coupled with the substrate temperature. In addition, they noted a much improved microstructure from growth at 950 °C versus growth in the 750 to 850 °C range and that the maximum growth rates occurred when the vapor composition was close to stoichiometric.

Kuwamoto (ref. 21) grew seeded CdTe by the effusive ampoule PVT technique with good results. He noted that the $(111)_A$ Cd face was preferable for epitaxial growth in the 680 to 850 °C temperature range. (As discussed in section 3.3, we have reasons to believe that his assignment of A and B faces is erroneous). In addition, he found poor lateral spreading of seed plates as well as void formation, probably because of the low substrate temperatures used. Lauck and Muller-Vogt (ref. 91) studied the incorporation of dopants in the effusive ampoule ("semi-closed ampoule") vapor growth of CdTe.

Closed ampoule vapor growth yields typically only small crystals with average transport rates of 1 to 2 g/day. Among the workers that used a closed ampoule vapor growth technique, Mochizuki et al. (refs. 76 to 80) performed extensive growth rate tests with overpressures of either Cd or Te and showed that the P_{min} condition leads to the highest growth rate. In an ingenious furnace arrangement Glebkin et al. (ref. 48) and Klinkova et al. (ref. 49) grew CdTe epitaxially on CdTe seeds (ref. 48) or on sapphire substrates (ref. 49) without ampoule wall contact and "without any temperature gradients in the bulk of the crystal" (refs. 48 and 50). Both obtained p-type crystals of up to 170 g with transport rates of 1 to 2 g/hr. EPD's were in the range of $10^4/cm^2$ (ref. 48). In addition Klinkova et al. varied the stoichiometry of the initial charge and found that the final crystals were always enriched with tellurium. For additional references on "contactless" growth see also (refs. 43 to 47). Golacki et al. (ref. 46) grew 8 mm diameter CdTe crystal also without ampoule wall contact utilizing various filling gases. However, their growth rates were only 1 to 2 g/day. Interesting their growth rates with hydrogen gas as a filling agent were twice those in vacuum. This may indicate that (1) there was a strong convective contribution to growth, and (2) that the initial charge was shifted from the congruent composition. Geibel et al. (ref. 81) grew twinned CdTe crystals that did not

adhere to the silica container after an in-situ reaction, purification and growth procedure. They also found that the crystals from experiments with the highest growth rates had the highest twin density, which they interpreted as a relationship between twin formation and stoichiometry. Yellin et al. (refs. 82 to 85), using unseeded vertical vapor growth with axial temperature gradients of 2 to 5 °C along the entire ampoule (5 to 10 cm) produced 15 g single crystals with an EPD of $2x10^3/cm^2$, with growth rates in the 1 to 2 g/day range. They found that the highest growth rates were obtained with slightly Te rich charges; however, in all cases the growth rates decreased during the course of an experiment. In addition they showed that the resistivity and carrier type could be varied depending on the stoichiometry of the initial charge; their highest reported resistivity was $2x10^9$ Ωcm.

2.3 ETCH PIT DENSITY DETERMINATION AND FACE POLARITY IDENTIFICATION

Brown (ref. 66) gives an excellent review of the etching behavior of CdTe and other physical properties important for growth. Traditionally, etch pit density (EPD) of CdTe crystals are determined with an etchant consisting of 3:2:2 parts of $HF:H_2O:H_2O_2$ developed by Nakagawa et al. (ref. 86). One should note, however, that Fewster et al. (ref. 87) showed, after much confusion in the literature, that this etchant pits only the Cd(111) face. Nakagawa et al. showed earlier that there was a one-to-one correlation between mechanically introduced dislocations, as revealed by this etchant, and dark spots obtained with cathode luminescence microscopy. However, they incorrectly identified the (111)Te face as being the etched face. In our own work, we have noticed that this etchant leaves the Te(111) face black. Other etchants in use are a lactic acid etch [II-VI Inc.], an additional lactic acid etch put forth by Meyers (referred to in ref. 88) and an acetic acid etch by Durose (referred to in ref. 88).

3. EXPERIMENTAL WORK UNDER THIS CONTRACT

3.1 DESIGN CONSIDERATIONS AND BASIC DESIGN

As outlined in section 1.1, an efficient development of optimum vapor crystal growth conditions requires some independence in the control of bulk and interfacial vapor transport fluxes from the adjustment of interfacial temperature conditions. Also a predetermined location for nucleation and growth as well as control over the number of nuclei is required. Closed ampoule technology, as exclusively used and planned for space experiments, allows for little control of these parameters.

Our design was based on the following basic considerations:

(1) To obtain defined, reproducible and rapid transport in vapor growth, gaseous impurities and excess components (see sect. 2.1), that can form transport limiting diffusion barriers at the growing crystal (see sect. 1.2.1), must be continuously removed.

(2) To reduce multiple or secondary nuclei formation and allow for some separation of the interfacial concentration and temperature gradients, an adjustable temperature "hump" between the crystal and source is required.

(3) To obtain steady growth conditions, the temperature difference ΔT_{sc} between source temperature T_s and crystal interface temperature T_c must be large as compared to temperature fluctuations inherent to the furnace-controller system ΔT_{contr}.

(4) To adjust the stoichiometry of the vapor, in order to produce semi-insulating or n-type material, an element reservoir needs to be provided. The temperature of this reservoir must be controlled independently from the other furnace regions (zones). Note, however that the fixing of partial pressures away from the congruent vapor composition, i.e., the presence of "excess components" (see (1) above) will reduce the transport rate, even under effusion conditions.

(5) To minimize the introduction of strain in the crystal during growth and cooldown, axial and radial temperature gradients should be reduced such that the induced stress does not exceed the stacking fault formation energy or the critical resolved shear stress. However, this condition cannot be quantified, since Young's modulus for CdTe is not known as yet.

(6) To obtain continuous growth, the ampoule needs to be continuously repositioned within the heating arrangement. However, individual furnace translation steps must be small enough, such that the product of discontinuities in displacement and temperature gradient about the crystal be much less than the difference in temperature between source and crystal surface temperatures, ΔT_{sc}, that drives vapor transport and growth.

(7) To (a) observe nucleation and consecutively lower the supersaturation to prevent concurrent nucleation and growth, (b) etch seed plates in a controlled way to prepare in-situ structurally unperturbed and chemically pure seed surfaces for optimal epitaxial growth, and (c) to monitor growth rates and morphologies, viewing of the crystal-vapor interface must be provided.

(8) To optimize the temperature control via a defined heat loss on the surface of the furnace shell, and for a safer operation, furnace shell cooling must be provided.

(9) To minimize the electric power requirements, an important consideration for spaceflight operation, a furnace design with high thermal efficiency is needed.

The above requirements have been accommodated in the basic design that is schematically depicted in Figure 2. Vapor transport and crystal growth is conducted in an ampoule that consists of three compartments: an element reservoir that is connected via a circular capillary to a source chamber, which, in turn, is connected via a second capillary to a growth chamber. The bottom of the growth chamber is flat to provide for better heat transfer from a seed to a supporting light pipe. In addition, in the vicinity of the seed, the growth chamber has leaks, of defined size, to a vacuum shroud that houses the ampoule arrangement. Note that, in addition to providing a means to establish rapid, diffusionless

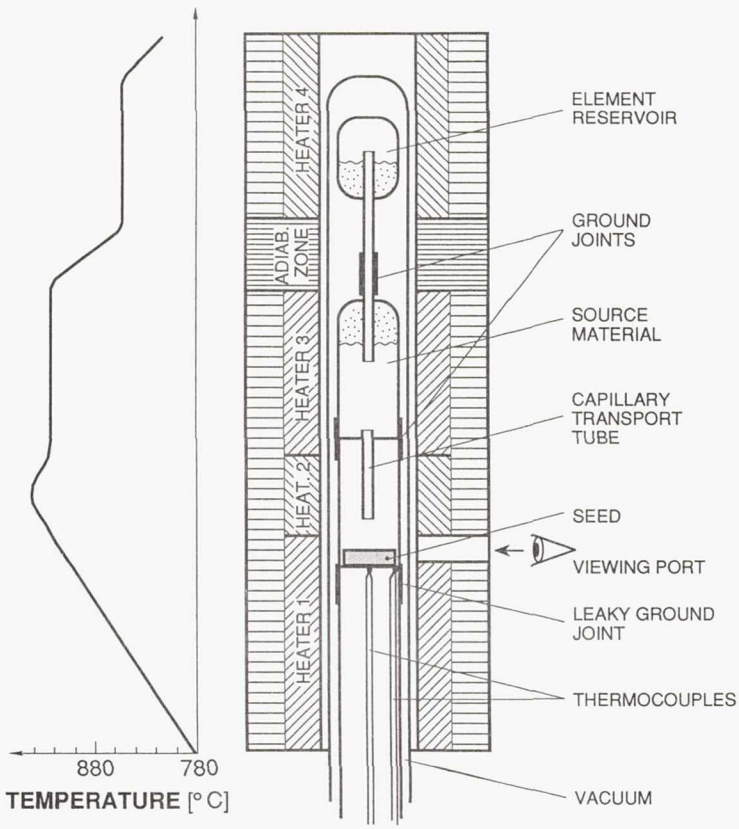

Figure 2.–Schematic presentation of the design features of the effusive ampoule physical vapor transport system and the idealized axial temperature profile. For details see text.

transport in the ampoule (see below), this vacuum shroud also reduces impurity diffusion from the heaters to the interior of the ampoule (ref. 28).

The circular capillary between source and growth chamber is dimensioned as follows. If the total pressure is such that collisions between vapor molecules dominate molecule-wall collisions (i.e., the Knudsen number is much less than 1) the flow is viscous and the transport rate can be predicted based on the Hagen-Poiseuille relation (ref. 92). In the usual form the Hagen-Poiseuille relation applies only to incompressible fluids, i.e., with constant density along the transport path. For an approximation of this condition, we assume that the vapor composition at the source and the capillary opening into the growth chamber are close to each other, i.e., that the stoichiometry of the vapor is not upset during transport, e.g., by nonequilibrium phenomena such as thermal diffusion. In addition, we introduce an average temperature $(T_s + T_c)/2$ and pressure $(P_s + P_c)/2$ in the capillary. Under this provision, and employing the ideal gas law, the number of moles flowing each second through a tube of radius r and length L is then (ref. 14)

$$N = \frac{a^4 \pi}{8 \eta L R} \frac{P_s^2 - P_c^2}{T_s + T_c} \qquad (1)$$

where η is the viscosity of the vapor and R is the universal gas constant. The applicability of equation (1) to diffusionless PVT has been experimentally confirmed (ref. 14).

For typical ampoule diameters and interfacial vapor pressures, equation (1) predicts transport rates that are too high for typical interface kinetics to result in structurally perfect single crystal growth, even at the smallest ΔT_{sc} that can be sustained with standard temperature controllers; for an example see reference 14. Note, however that the transport rate scales with the fourth power of the tube radius or diameter. This strong dependence can be advantageously used for an optimal effusive PVT ampoule design, following these practical considerations:

Given a furnace-temperature controller system with a certain ΔT_{contr}, in order to ensure steady transport and growth (see (3), above) one will maintain a $\Delta T_{sc} >> \Delta T_{contr}$. Practically, this ΔT_{sc} can be realized only over a certain distance that roughly determines the capillary length L. In our example, the magnitude of L is given by the width of the independently controlled "temperature hump" of heater 2 in Figure 2. From kinetics considerations or experience, one chooses T_c and the magnitude of the vapor flux N that can be accommodated at T_c in a single crystal growth mode. After choice of a specific ΔT_{sc}, T_s is given. Assuming equilibrium vapor pressures, the temperatures T_s (heater 3) and T_c (heater 1) determine the pressures P_s and P_c. Assuming that the viscosity of the vapor is known (for estimation methods see, e.g., sect. 5.3.3 in ref. 22), equation (1) can then be solved for the desired capillary diameter.

The size of the effusion holes (leaks) is chosen such that a volume flow of about 10 to 15 percent of N is established into the vacuum shroud. This suffices, according to our earlier experience (refs. 14, 18, and 19), to establish diffusionless transport, in which the transport rate is limited only by viscous interaction of the vapor flow with the capillary wall - a necessary condition for the applicability of equation (1).

The dimensions of the capillary between element reservoir and source chamber are chosen according to yet another set of considerations. The element vapor pressure needed for stoichiometry adjustment is typically so low that, as indicated in the idealized temperature profile in Figure 2, the temperature of heater 4 is several hundred degrees lower than those of heaters 1 to 3. (Note the adiabatic zone in the heater arrangement, that is to facilitate establishment of this large temperature difference over a reasonably short distance). Consequently, the source material will tend to also condense in the element reservoir or, even worse, in the capillary. This, however can be prevented, by choosing the diameter of the capillary small enough that the flow velocity of the element vapor towards the source chamber overrides the diffusion velocity of the CdTe vapor constituents in opposite direction. One can base an estimate of this flow velocity, for

instance, on the assumption that a certain percentage of the vapor losses through the leaks from the growth chamber consist of element vapor that must be replenished from the element reservoir.

Besides the above features, the basic design provides for:

- viewing of the seed/crystal interface,
- relative motion of heater arrangement (furnace) and ampoule/vacuum shroud, and
- cooling of the furnace shell.

3.2 EXPERIMENTAL APPARATUS

Figure 3 gives an overall photographic view of the crystal growth furnace and components. Figure 4 is a functional diagram showing the major system interconnections. The numbers for components in the overlay of Figure 3 and in Figure 4 are also used in parentheses in the following sections, and in the Suppliers List, appendix 2. The {bracketed} letters refer to the corresponding engineering line drawing in appendix 3. Drawing {A} presents the assembly and overall dimensions of the furnace cage. Appendix 4 lists major component dimensions, and requirements for power, cooling, vacuum, and gas-backfilling.

3.2.1 System Components

3.2.1.1 Heating arrangement and control. - The furnace (1), as schematically shown in Figure 2, consisted of four independently controlled heater zones with an adiabatic zone between zones 3 and 4. Detailed dimensions of these elements and of the insulation are presented in the heat transfer model that is presented in appendix 1. The furnace elements consist of Kanthal A-1 wire windings on alumina supports. The temperature of each zone, measured with a type-R thermocouple (2), is controlled by a 15-bit digital temperature controller (3) with an SCR power controller (4). Considering measuring and computational errors, the actual operation range of the controllers is 12 to 13 bit, resulting in a resolution of 1 part in 8200. Correspondingly, we obtained a temperature stability of $\pm 0.1\ ^{\circ}C$. These controllers were connected via a RS232/485 interface (5) to a dual serial port (6) of a personal computer (7) to provide both programming/control and monitoring capability. The rms voltage and current values of the SCR's were monitored through an A/D interface card (8) mounted in the computer. Front mounted panel meters (9) were also used to visually monitor the rms current and voltage for early detection of potential heater failures.

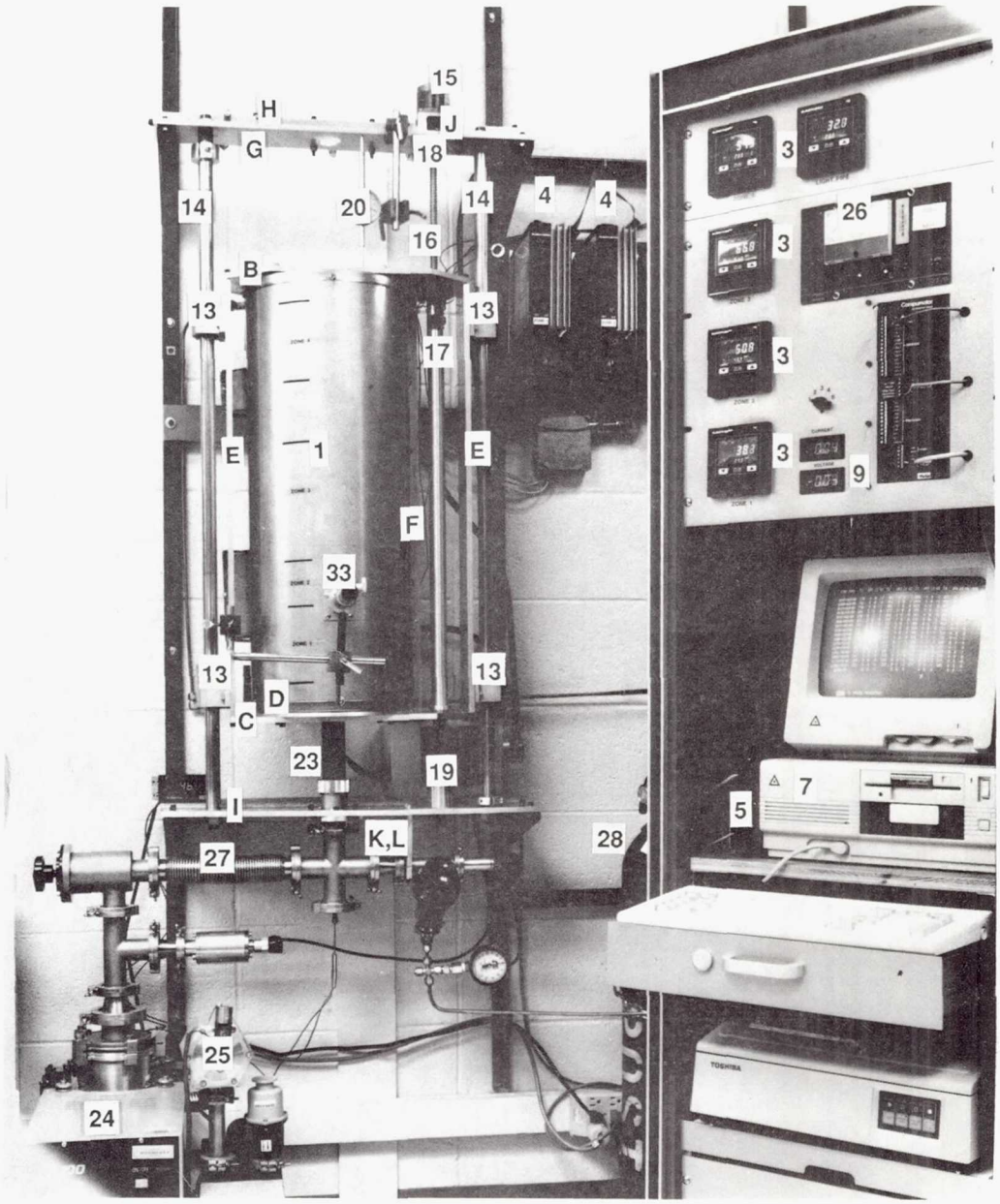

Figure 3.–Overall view of the effusive ampoule physical vapor transport system. Numbers and letters on overlay correspond to those used for the components in the text, see Sect. 3.2.

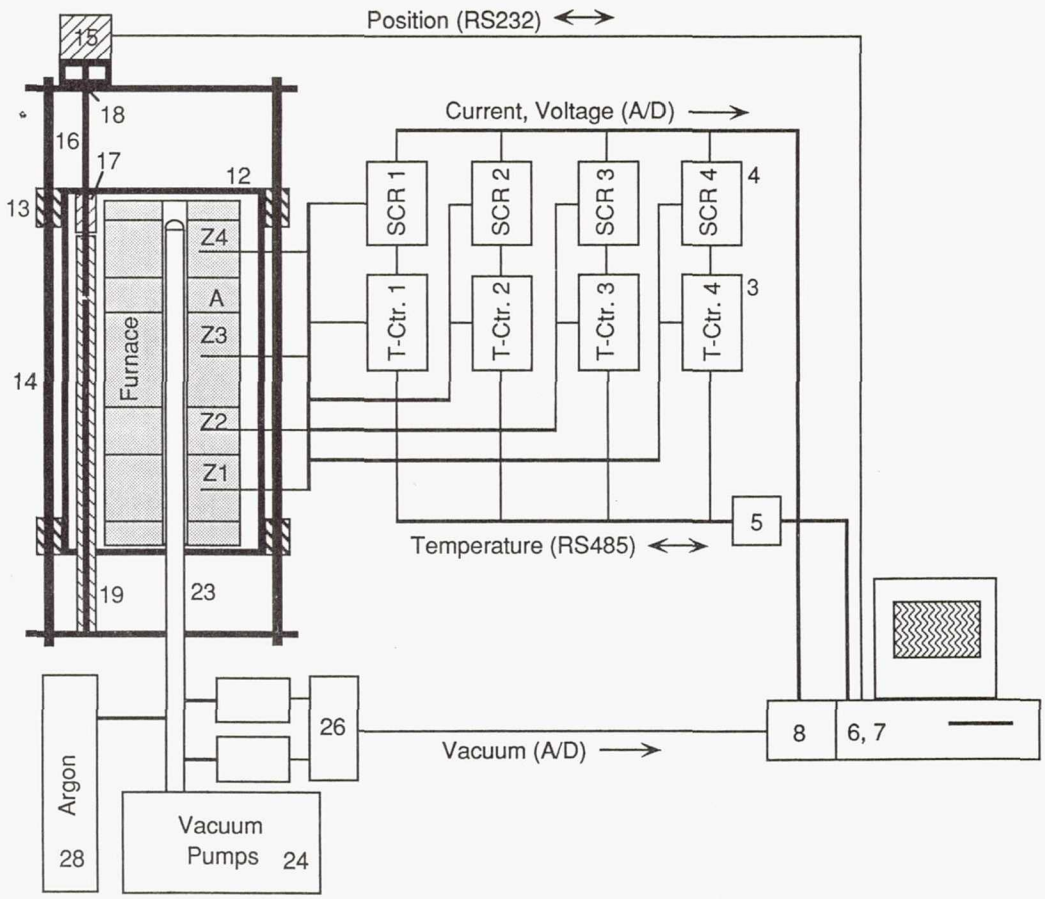

Figure 4.–Functional diagram showing system interconnections. Numbers correspond to those used for the components in the text, See Sect. 3.2.

Direct microscopic monitoring of the seed and the growth process is facilitated by two opposite viewing ports that are covered with gold coated quartz windows (10) to decrease infrared radiation losses.

The outer furnace shell temperature was maintained below 25 °C by water flow through copper cooling coils that are bonded (11) to the inner furnace shell.

3.2.1.2 Furnace support and motion. - The furnace is held in an aluminum cage (12) consisting of a top {B} and bottom {C} plate, ring {D}, two side plates {E}, and a back plate {F} for mounting the thermocouple terminal blocks. Four pillow block ball bearings (13) attached to the side plates allow for linear translation along ground shafts (14) that are supported by a top support plate {G} and bar {H}, and a bottom {I} support plate. These support plates are mounted onto wall brackets.

The furnace motion is controlled by a stepper motor (15) which, in turn, is controlled via a RS232 serial communication port from the system computer. The stepper motor is mounted on a standoff {J} and turns a lead screw (16) which is supported by a thrust type bearing (18) mounted in the top plate. Below that, the lead screw is attached to the furnace cage with a ball nut and flange (17). The resulting translation resolution is about 0.5 μm per motor step. A long custom wound spring with a low force constant (19) counterbalances the furnace weight.

The furnace displacement is measured with either a precision dial gauge (20) or an optical displacement measuring system consisting of a high pointing stability He-Ne laser (21) mounted to the support bar and a PIN linear photodiode (22) attached to the furnace.

3.2.1.3 Vacuum system. - The high vacuum in the vacuum shroud (23) is supplied by a turbomolecular pump (24) backed by a rotary mechanical pump. A solenoid valve (25) provides protection from oil backstreaming into the turbomolecular pump during a power failure and allows the vacuum pumps to be isolated from the vacuum shroud during backfilling with argon gas. The vacuum is monitored with a combined convection/penning gauge (26) with separate gauge heads for low and high vacuum. The vacuum system is connected to the vacuum shroud with ISO-40 stainless steel piping and fittings (27). Mounting brackets {K and L} are used to help support the various vacuum components.

An argon gas cylinder (28), connected to the vacuum system through a valve, allows for backfilling with dry gas before the removal of ampoules.

3.2.1.4 Ampoule construction and pedestal/crystal cooling. - Since in the EAPVT technique no ampoule sealing is required, the growth ampoule can be constructed from demountable ground joints. This facilitates the loading of source material and seed plates as well as the harvesting of crystals. All ampoule components were constructed of low OH^- concentration silica glass (23).

All crystal growth runs conducted under this Grant were performed without element reservoir. Hence, a growth ampoule consisted of only three ampoule sections:

- the source reservoir (29a), that connects with its ground joint to the
- the middle section (30), which houses the transport limiting capillary, and forms with
- the pedestal/cooling section (31) the growth chamber.

These parts are depicted in Figure 5 and schematically shown in figure 2. The source reservoir has a bulbed glass rod at the top to mechanically hold the compacted CdTe in place; for filling procedure see section 3.2.2. This is necessary because the effusive ampoule design appears to remove oxygen in the CdTe to an extent that, in combination with the low OH^- silica glass used, sticking to the silica walls is prevented. Thus, without this retaining rod the compacted CdTe would readily slide down the source reservoir, thereby

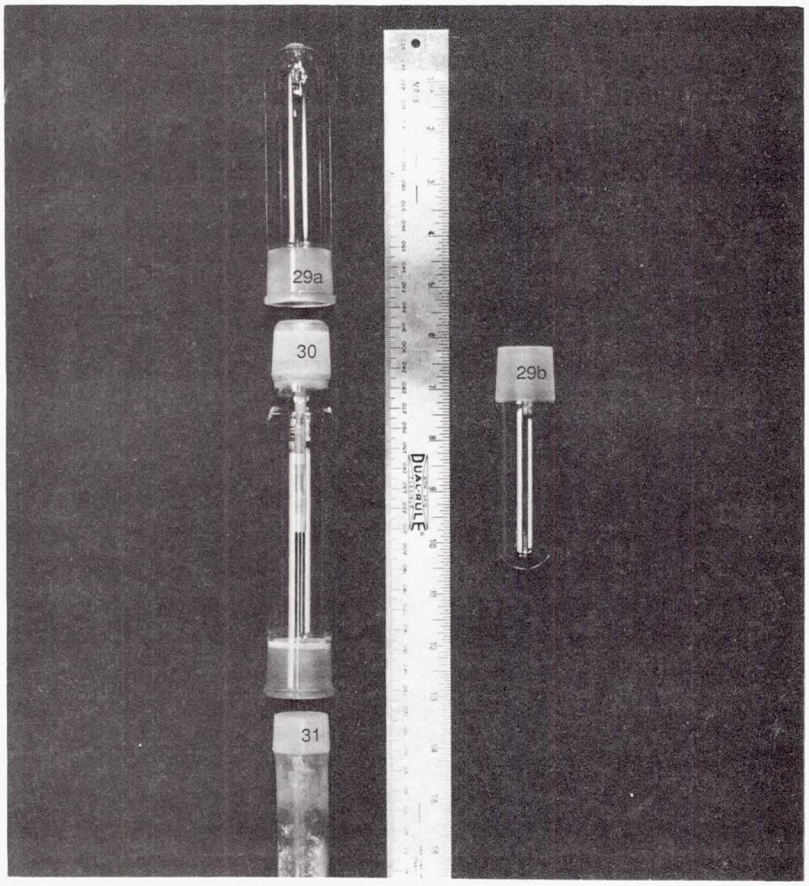

Figure 5.–Components of the silica ampoule. Numbers as used in text.

repositioning itself within the temperature profile, which would jeopardize control of the growth process.

Two geometrical variations of the pedestal/(seed/crystal) cooling section were employed. In one configuration, a 12 in. long 12 mm o.d. silica rod, which acts as a light pipe, was flared and then fused into an inner ground joint. The upper face of this pedestal was ground flat. The other end of the light pipe rested in a cupped aluminum rod that acted as a thermal conductor to room temperature, and provided a vacuum seal. In the other configuration, a silica plate was fused to the top of an inner joint, which, via a tubular extension formed the pedestal section. The end of the pedestal rested on a flange plate fitted with two 1/16 in. i.d. vacuum thermocouple feedthroughs. The thermocouples (4), contacting the underside of the pedestal at its edge and center, respectively, provided insight on the radial temperature distribution in the seed/crystal region. Their temperatures were monitored separately from the furnace heating elements.

The leaks in the vicinity of the growing crystal were introduced through the grinding of 2 to 4 facets of predetermined size on the side of the male ground joint of the pedestal. These facets were dimensioned such that under CdTe growth conditions up to 20 percent of the vapor that flows from the source reservoir to the growth chamber is lost to the vacuum shroud.

In addition to the three ampoule sections introduced above, a starting material section, (29b) in Figure 5, was used in the initial compacting of the source material into the source reservoir section (29a); for procedure see below.

3.2.1.5 Viewing. - Etching and growth of the crystal were monitored through the gold-coated windows (3) with either a long focal length microscope (33) with a reticle, or a compact CCD video camera (34).

3.2.1.6 Computerized system operation. - A personal computer (9) was used to control and monitor:

- the temperatures of the four heater zones,
- the rms currents and voltages of the heater zones,
- the vacuum/pressure in the shroud, and
- the stepping motor.

The interface cards employed are specified in the respective sections above. A BASIC language computer program that we developed in house was used to control and monitor the system operation.

3.2.2 Operation and Growth Procedure

3.2.2.1 Cleaning of the silica parts. - Prior to each run the silica glassware including the vacuum shroud was cleaned with aqua regia and rinsed several times with deionized water and finally reagent grade methanol or ethanol. The assembled components were then heated to 900 or 1000 °C (depending on the planned growth conditions) for 4 to 8 hr under a vacuum and then cooled. The components were then removed for immediate use or stored under nitrogen.

3.2.2.2 Starting material transport and compaction of the source material. - A bottom reservoir section (29b in fig. 5) filled with approximately 100 g of high purity CdTe (35) was joined to the source reservoir (29) and positioned in the furnace on a silica support tube such that the bottom of the reservoir appeared in the viewport. The vacuum shroud/ampoule was then evacuated for several hours before the furnace was ramped (at about 2 °C/min) to the transport temperatures, typically, 725, 700, 600, and 500 °C for zones 1 to 4, respectively. After transport was complete, typically within 24 hr for 100 g of CdTe, the furnace temperatures were adjusted to 800, 825, 650, and 600 °C for 24 to 48 hr to allow the source material to compact. The ampoule was then cooled to room temperature at about 1 °C/min. This low cooling rate is necessary to prevent cracking of the source reservoir, particularly the top rod and ball.

3.2.2.3 In-situ nucleation and growth. - In-situ nucleation and growth experiments were conducted in order to determine:

- the minimum temperature required to obtain isotropic growth, and
- whether single crystals could be obtained without introduction of seeds.

For in-situ nucleation and growth a previously cleaned and baked-out ampoule (pedestal and middle section) were combined with a source reservoir containing previously compacted material, and inserted into the vacuum shroud. After evacuation of the shroud, the system was evacuated. The furnace zones 1 to 4 were ramped to temperatures of 820, 880, 850, and 750 °C, respectively, (or alternatively 780, 820, 800, and 700 °C) at 5 °C/min. Note that, because the crystal is between zones 1 and 2 its temperature is then approximately 850 °C. At this point the source temperature (zone 3) was increased in discrete steps of 1 or 2 °C until nucleation was observed. Typically 3 to 5 nuclei were present. We did not succeed in reducing their number to the desirable single nucleus through consecutive thermal etching. At this point the source was ramped to approximately 880 °C, (where growth rates of 5 mm/day are obtained) and the crystallites were allowed to grow until they covered the pedestal. The vacuum shroud was then backfilled with 100 to 300 torr of argon gas and ramped down to room temperature at 1 °C/min.

3.2.2.4 Seeded growth. - Seeded growth runs were conducted with seeds obtained from either unseeded runs (smaller seeds, close to [110] orientation) or with commercially obtained seeds (35), typically of [111] orientation.

Seeds from unseeded runs were only rinsed with methanol prior to use. Commercially obtained seeds were characterized with respect to their face type (see sect. 3.3) and then lightly polished with a 2 percent Br_2/ethylene glycol solution and rinsed in methanol. In later runs the final rinse was a 25 percent HCl solution, followed by a rinse with deionized water to make the seeds hydrophobic (ref. 66).

After placement of a seed on the center of a pedestal section, an ampoule with source material in the source section was assembled and placed into the vacuum shroud. Most seeded runs were conducted with an initial backfill of a few torr of argon gas. Then the furnace zones were ramped to 890, 910, 903, and 850 °C (or 835, 865, 850, and 800 °C) respectively at 0.5 to 0.75 °C/min. Once the above temperatures were reached the vacuum was started. However, some runs were conducted entirely under vacuum. After the seed had slightly etched the source zone was ramped to 920 °C at 0.1 to 0.02 °C/min. When the crystal had completely filled the pedestal and had stopped growing in height, typically 12 to 24 hr after the source reservoir zone ramping was started, the furnace motion was started. Typical translation rates were 0.5 cm/day, although rates as high as 1.2 cm/day were explored.

On completion of the run, after 1 to 3 days, the ampoule was backfilled with a few torr of argon gas and the furnace was ramped down to room temperature at 0.2 to 1 °C/min.

3.2.2.5 Etch pit density and face polarity identification. - For the determination of etch pit densities (EPD) we used the Nakagawa etch (ref. 86). For Cd/Te (A/B) face identification we used three "black and white" etchants. They were a lactic acid etch used by II-VI Inc., an additional lactic acid etch due to Meyers and an acetic acid etch due to Durose (for references on both see ref. 88). All turned the Cd(111) face black and left the Te face shiny. Finally we opted for the II-VI etchant because it was less violent than

Brown's et al. etch and it uses much less HE acid than both other etches. However, it should be noted that a slight amount of agitation is necessary for the II-VI etchant to work.

For crystal polishing we chose a 2 percent Br_2/ethylene glycol solution (ref. 89). Chemical polishing probably damages the CdTe surface less than mechanical polishes, which typically have to be followed by a 5 percent Br_2/MeOH etch to remove the surface damage. We have found that there is no change in the EPD when crystals polished in 2 percent Br_2/ethylene glycol are etch in 5 percent Br_2/OH; for a study of mechanical polishing damage see reference 90.

4. RESULTS AND DISCUSSION

4.1 VAPOR CRYSTAL GROWTH TECHNOLOGY

We have successfully developed a novel vapor crystal growth furnace and ampoule system in which grow rates of 1 cm/day are achieved and sustained (depending only on the amount of source material), with temperature differences between the source and the crystal of 2 percent of the working temperature (i.e., 20 K at 1173 K). This indicates that impurities with high vapor pressure (fugacity) are removed preferentially during both source transport/compaction and growth. The compacted source material does not adhere to the ampoule even without special (carbon) coatings. This indicates that the low vapor pressure impurities (i.e., oxides) are preferentially left behind in the starting material during the transport and compacting process.

The furnace operated very efficiently, requiring only 150 W for steady state operation at 900 °C. In addition water cooling between the inner and outer shells maintained the outer shell at or below room temperature, providing for safe operating conditions.

The furnace heating (i.e., ramping) and translation were controlled via a user-friendly BASIC language program from a personal computer, which also monitored various other furnace and operating system parameters and displayed them in a useable format. With the PC and interconnected temperature controllers the temperatures were stabilized to $\pm$0.1 °C and ramping rates as low as 0.01 °C/min were executed.

The heat transfer and resulting temperature distributions in the furnace were modeled using the numerical code SINDA (ref. 93). In runs without an ampoule inside the vacuum shroud, good agreement between experimental and numerical shroud temperatures were obtained. Preliminary numerical runs with an ampoule agreed well with the limited experimental data available. Therefore, a realistic thermal model of the entire system can probably be obtained using this code. It has been reported to us that this is the first experimental verification of SINDA results. A full description of the heat transfer model and results are given in appendix 1.

The use of viewports to monitor crystal growth proved to be only partially successful. The viewports allowed for determinations of the temperature differences (supersaturation) required for nucleation and growth, and the observation of growth patterns. Also, viewing is essential for a controlled thermally etching of seeds prior to growth. In addition, we were

able to monitor the actual crystal growth rates versus the furnace translation rates. However, the view ports introduced a strong (up to 10 °C/cm) radial asymmetry in the temperature distribution. This caused crystals to attain a saddle shape, with the highest part towards the viewports. Yet, secondary nucleation could not be detected in the final crystals. This problem can be readily alleviated in future designs by either increasing the power density around the (decreased size) view ports, or geometrically more advantageous viewing through high temperature fiber arrangements.

4.2 CADMIUM TELLURIDE GROWTH

4.2.1 In-situ Nucleation and Growth

We found that there is no pronounced growth rate anisotropy for CdTe in the 800 to 900 °C range. In-situ nucleated crystallites spread laterally uniformly and vertical growth became significant once the polycrystalline layer had reached the ampoule wall. Small crystals (less than 2 mm) were faceted although larger crystal rarely showed faceting.

We found it impossible though to obtain in-situ nucleation of a single crystal even with radial temperature gradient that were estimated 10 °C/cm. There were always three to five nuclei present. Also it was not possible to reduce this initial number by either crowding-out, since all nuclei grew at the same rate, or by thermal etching. By x-ray diffraction analysis it was determined that most of the crystallites grew approximately in the [110] direction. The final polycrystals typically had 10 grains that were arranged in a radial pattern.

The grown crystals never adhered to the GE 214 silica (23) regardless of the surface preparation (e.g., rough finish, fire polished). This coupled with the nonadhesion in the source reservoir leads us to believe that we effectively remove oxides which are known to adhere to silica glass.

4.2.2 Seeded Growth Runs

We attempted to epitaxially grow CdTe on [110], $[111]_{Cd}$ and, $[111]_{Te}$ seed plates. In most cases the resulting crystals had low angle grain boundaries and were twinned. In one case, the final crystal was at least 90 percent (twinned) single crystalline. Typically, lateral growth on the seed plates occurred without twinning and grain boundaries. These defects formed mostly in higher areas of the crystal. This is likely due to the strong radial and axial temperature gradients that existed in the system.

Growth rates were 0.5 to 1.2 cm/day (at 25 mm O.D.). Sticking became a problem with the seeded runs and added to the twinning and low angle grain boundaries. At this point it is unclear whether this was due to water in the argon gas used for backfilling or whether it was due to oxides present in the seeds themselves. Typical EPD's were $2x10^3/cm^2$. This is among the lowest values reported and may be due to either the low oxide concentrations in the crystals or to reduced mechanical interaction with the ampoule walls. The room temperature resistivity was 9.8 Ω cm, hall mobility was 76 cm^2/Vsec and

the material was p-type with a carrier concentration of 8.4×10^{15} cm^{-3}. Further tests are required to determine the exact carrier type. The optical transmission was about 62 percent between 860 nm and 32 μm. The theoretical values for this range is only about 63 percent (refs. 66 and 72), due to the high refractive index of CdTe. No additional peaks were found in the transmission/absorption curves. These results are indicative of high purity material. Large areas (0.5 to 1 cm^2) were precipitate free as determined by infrared microscopy performed with a Leitz research microscope and a lead sulfide tube camera (36). Precipitates were primarily noted along twin and grain boundaries.

ACKNOWLEDGMENTS

Support of this research by the National Aeronautics and Space Administration under Contract NAS3-25361 and by the Boeing Aerospace Company under Contract HD 6763 are gratefully acknowledged. In addition, the State of Alabama has supported this work through the Center for Microgravity and Materials Research at the University of Alabama in Huntsville. We would also like to thank the II-VI Corporation for their technical assistance in the characterization of samples and supply of seed plates. This work has also greatly benefitted from numerous discussions with Dr. Margaret Brown of the Grumman Corporation. Expert machining by the UAH machine shop under the supervision of Mr. Vince Provenca and exemplary glassblowing by Mr. Anthony Nelson were essential for the success of this project.

APPENDIX 1 - HEAT TRANSFER MODEL

The heat transfer in the furnace was modelled based on the numerical code SINDA (ref. 93). The numerical work was carried out by P.N. Galloway under the supervision of Prof. F.C. Wessling of the Mechanical Engineering Department of UAH. In the following we will briefly outline the model and present the results. For more details it is referred to the Master Thesis of P. Galloway (ref. 94). The following assumptions were made to model the heat transfer in the furnace; see also Figure 6.

(1) Radiative heat exchange occurs between the inner heating element surfaces and the silica vacuum shroud, and across the shroud.

(2) Conductive heat transfer occurs along the heating elements, and along and across the shroud wall. Conduction also occurs across the insulation between the heating elements and the inner shell, across the unheated end zones and, across an insulation plug above the vacuum shroud. Uniform contact resistances are assumed between the individual zones.

(3) Convective heat transfer occurs from the cooling coils bonded to the inner furnace shell to flowing water, and between the heating elements and the shroud.

(4) Power densities in the heating zone are individually uniform.

(5) The viewports and their effect on the heat transfer are ignored.

The mesh used in the computations was chosen to allow for maximum flexibility while conserving computation time. Figure 6 gives a half cross-sectional view of the axisymmetric mesh. Coarse grid spacing was used in the insulated region between the heating elements and the inner shell where conduction is the primary heat transfer mode. A finer mesh was used for the heating elements which consist of an outer alumina support and Kanthal A-1 wire windings embedded in a high temperature cement. The shroud has nodes only on each of their surfaces. The dimensions were supplied by the furnace manufacture.

This model was used to determine the temperature distribution on the inside wall of the shroud and the heat losses to the cooling water, with the experimentally determined steady-state power for each zone as the input parameter. Variations of thermal and optical material properties with temperature were accounted for.

The model was used to obtain either:

- temperature profiles on the inside wall of the vacuum shroud for given input powers, or
- input powers required to obtain a certain temperature profile.

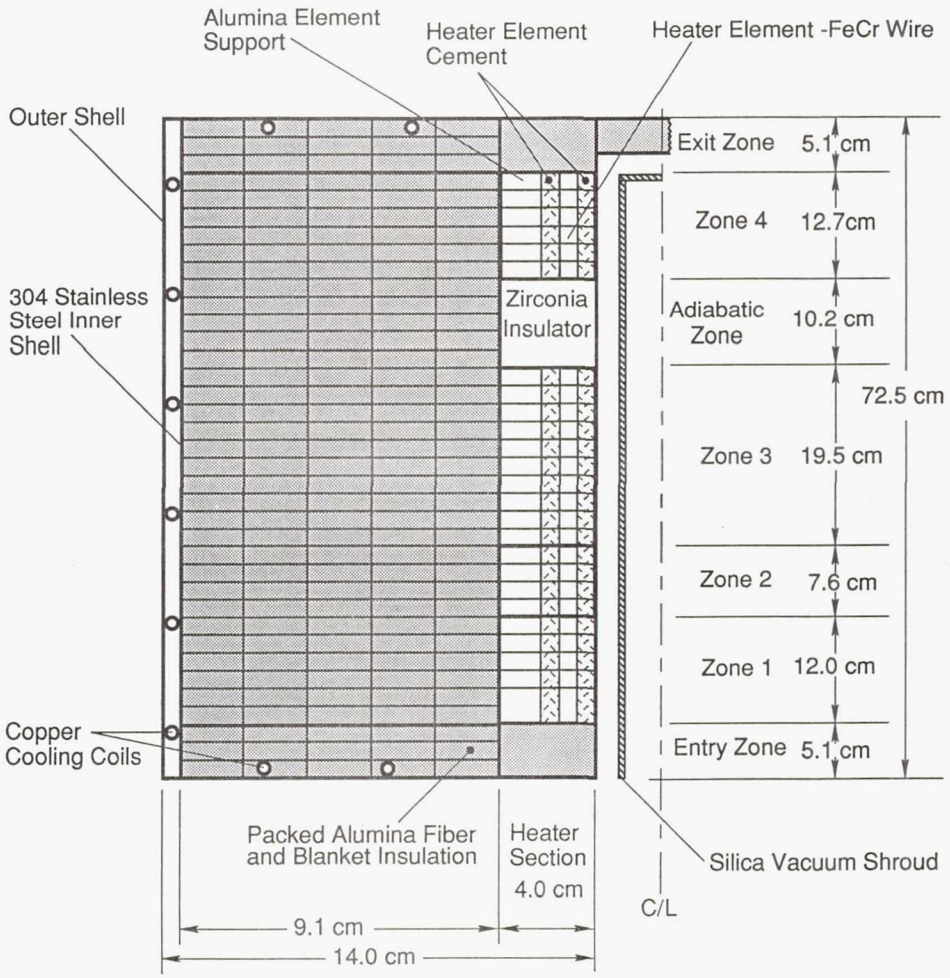

Furnace Heat Transfer Model

Figure 6.–Schematic presentation of half cross-section of the furnace and vacuum shroud used in the axisymmetric heat transfer model. Grid shown corresponds to the computational mesh used.

In the first group, experimentally determined input powers to obtain either 900 °C or a target temperature distribution at the four control thermocouples (see table I) were two profiles. For the constant temperature case the experimental and numerical input used. In the second group, the numerical input powers were varied to reproduce these powers agreed within 1 percent. Figure 7 shows the corresponding numerical and experimental temperature profiles. In Figure 8 we have plotted the experimental and numerical temperatures resulting from the experimentally determined input powers (fourth column in table I) for the target profile. Overall, reasonable agreement is obtained, although there are deviations in temperature of up to 10 percent in zone 1. The deviations in zones 2 to 4 are 5 percent or less. For Figure 9 the numerical power inputs have been adjusted to obtain a better fit between the experimental and numerical temperature profiles at the locations of the control thermocouples. The adjusted input powers are listed in the next to last column in table I. One sees that numerical and experimental power inputs differed individually by up to 12 percent, yet the total power differed only by 1 percent.

In summary, this work showed that the SINDA code can be used to predict furnace/shroud temperatures reasonably well. However, as in all models, only accurate and complete accounting of the thermal and physical (construction) parameters of the furnace and its materials will lead to high fidelity.

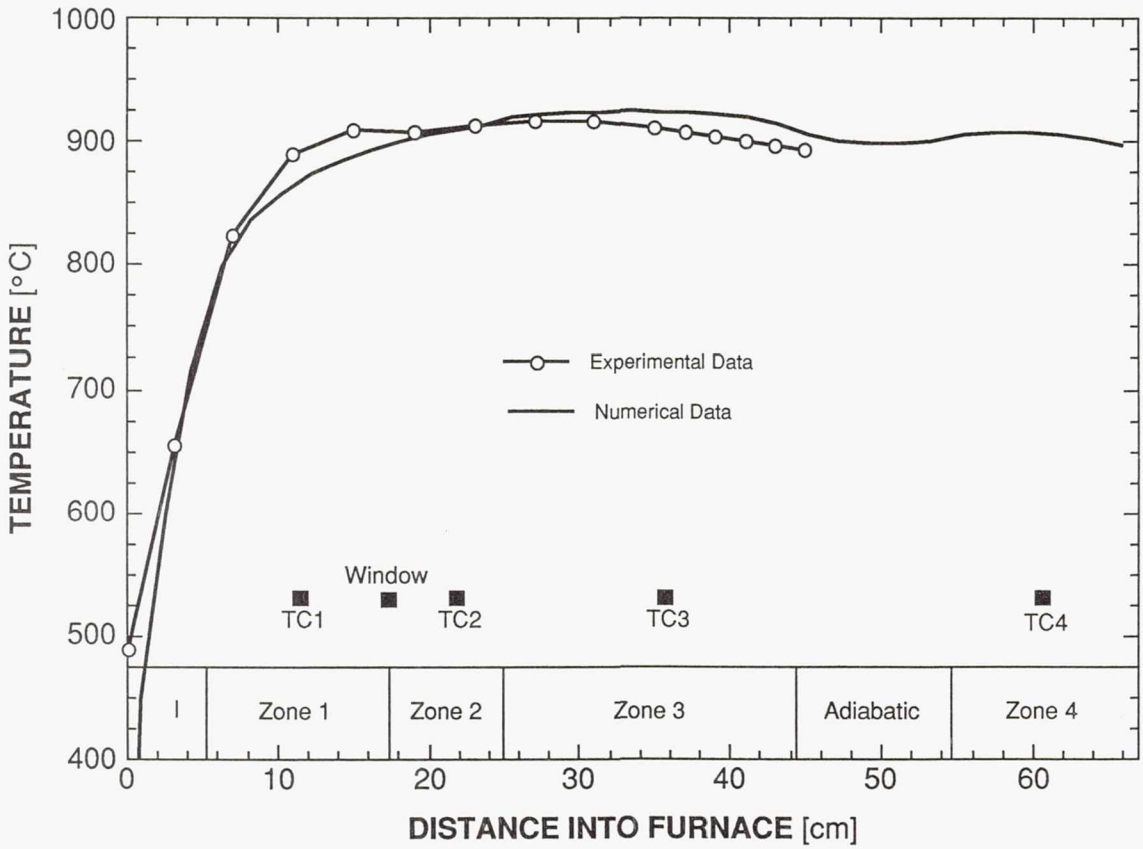

Figure 7.–Comparison of experimental and numerical axial temperature profiles for the case that all four control thermocouples are at 900 °C. Numerical input powers into the four heated zones are equal to the experimental values.

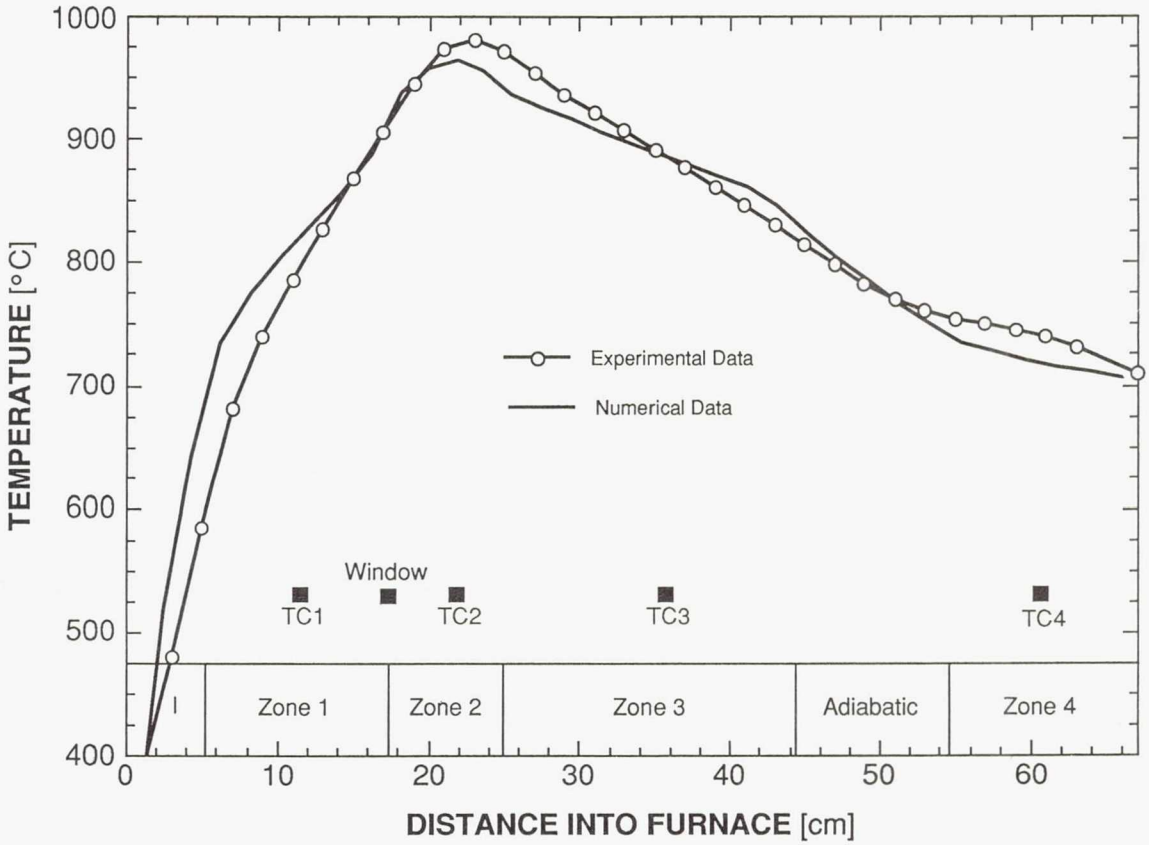

Figure 8.–Comparison of experimental and numerical axial temperature profiles for the target temperature distribution. Numerical input powers into the four heated zones are equal to the experimental values, see Table 1.

TABLE I. - TEMPERATURES AND POWERS REQUIRED IN HEATING ARRANGEMENT

Zone	Uniform 900 °C, input power, W	Target temperature distribution input power, W			
		Temperature, °C	Experimental	Numerical	Difference, percent
1	67	775	18	15.8	-12
2	20	1000	90	94.5	5
3	45	925	24.2	22.3	-7.9
4	26	725	12.8	13.8	7.8
Totals			145	146.4	1

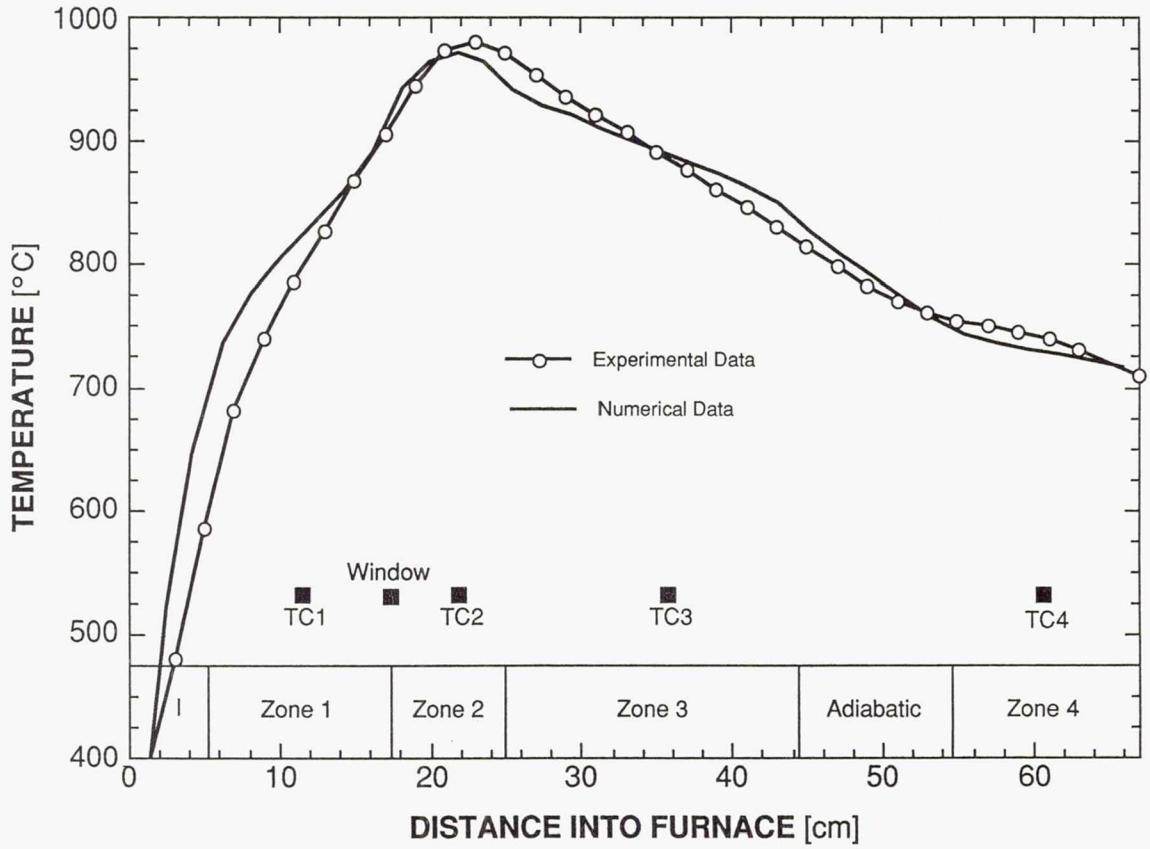

Figure 9.–Comparison of experimental and numerical axial temperature profile for the target temperature distribution. Numerical input powers into the four heated zones have been adjusted to obtain a closer fit to the experimentally obtained profile, see Table 1.

APPENDIX 2 - PARTS LIST AND SUPPLIERS

(1) Furnace, four heated zones with Kanthal A-1 elements, custom fabricated, Thermcraft Inc., Winston-Salem, NC 27117

(2) Thermocouple wire, type R, 0.020 in. diameter, Omega Engineering, Stamford, CT 06906

(3) Digital temperature controller, model 818P, Eurotherm Corporation, Matthews, NC 28105 (Mr. Thomas Avis)

(4) Power controllers, SCR, model 461-15A-120V, Eurotherm Corp, Matthews, NC 28105 (Mr. Thomas Avis)

(5) Serial Interface, model 261, Eurotherm Corp, Matthews, NC 28105 (Mr. Thomas Avis)

(6) Dual serial port, model SPC20-OPT, Industrial Computer Source Book, San Diego, CA 92123

(7) Personal Computer, model D, Leading Edge Corp, Needham Heights, MA 0219

(8) Analog-Digital I/O Card, model AI08-B, and Analog Multiplexer, model AT-16, Industrial Computer Source Book, San Diego, CA 92123

(9) LED Panel Meters, model DP-354, Acculex, Taunton, MA 02780

(10) Quartz disks, 1/16 in. thick, Quartz Scientific, Fairport Harbor, OH 44077. The gold coatings were prepared by personnel in the UAH Center for Applied Optics

(11) Aluminum putty, Type (F), Devcon Corp., Danvers, MA 01923

(12) Aluminum jig plate, 3/8 in. thick, Tull Metals, Birmingham, AL 35204

(13) Pillow block bearings, model SPB-l6ADJ, 1 in. nominal shaft diameter, Thompson Industries, Port Washington, NY 11050

(14) Case hardened ground shafts, class "L," 48 in. long, Thompson Industries, Port Washington, NY 11050

(15) Stepper motor, model AX5751, Compumotor, Parker Hannifin Corp., Peteluma, CA 94952

(16) Leadscrew, ball nut and flange, model R-0505, Warner Electric, South Beloit, IL 61080

(17) Flexible shaft coupling, model BT0075-C.1250-C.250, 0.25 in. diameter, Racom Corp., Huntington Beach, CA 92649

(18) Flange bearing, model Z97, Bardeen Corp., Danbury, CT 06813

(19) Spring, custom wound, spring constant 3 lb/in., relaxed length 67 in., Associated Spring, Corry, PA 16407

(20) Swiss precision dial indicator, 50 mm travel x 0.01 mm resolution, Timesaver Industrial, Salt Lake City, UT 84119

(21) He-Ne Laser, model 1303P, 2 mW, Uniphase Corporation, San Jose, CA 95134

(22) Photodiode, model SL-76, United Detector Technology, Hawthorne CA 90250

(23) Silica Tubing, type 214, General Electric Corp., supplied by National Scientific Inc., Quakertown, PA 18951

(24) Turbomolecular pumping package, Alcatel model AV95001, supplied by Kurt Lesker Co., Clairton, PA 15025

(25) Vacuum sentry safety valve, model 145-0025K-120 V/60 Hz, HPS Corp., Boulder, CO 80301

(26) Combined Convection/Penning gauge, Alcatel model 96012, supplied by Kurt Lesker Co., Clairton PA 15025

(27) Vacuum components, ISO-40 (Universal), HPS Corp., Boulder, CO 80301

(33) Telemicroscope, model Ml01AT, Gaertner Scientific Corp., Chicago, IL 60614

(34)* Video Camera, model Elmo EM-102BW, Elmo Mfg. Corp., New Hyde Park, NY 11040

(35) CdTe, high purity; CdZnTe, transmission blanks; II-VI Inc., Saxonburg, PA 16056

(36)* Lead sulfide camera tube, Vashaw Scientific, Norcross, GA 30092

*Purchased with funds from the State of Alabama through CMMR, UAH.

APPENDIX 3 - PHYSICAL DIMENSIONS AND REQUIREMENTS

Furnace:	11 in. o.d. x 29 in. length
Furnace plus support elements:	46 in. height x 25 in. width x 16 in. depth
Power requirements:	158 W total for operation at 900 °C, zone 1 requires approx: 67 W, zone 2: 20 W, zone 3: 45 W, and zone 4: 26 W
Cooling requirements:	3 liters/min at 25 °C for a water temperature increase of 1.5 °C
Vacuum requirements:	Overall vacuum pressure of less than 0.1 torr, hydrocarbon free
Gas filling requirements:	2 liters at 1 atm (during cooldown)

APPENDIX 4 - ENGINEERING DRAWINGS

{A} Assembly of furnace cage and support plates

{B} Furnace cage top plate

{C} Furnace cage bottom plate

{D} Furnace ring support

{E} Furnace cage side plate

{F} Furnace cage back plate

{G} Top support plate

{H} Top support bar

{I} Bottom support plate

{J} Stepper Motor Mount

{H} Split collet for vacuum valve support

{L} Split collet for vacuum port interface

Assembly of Furnace Cage and Support Plates

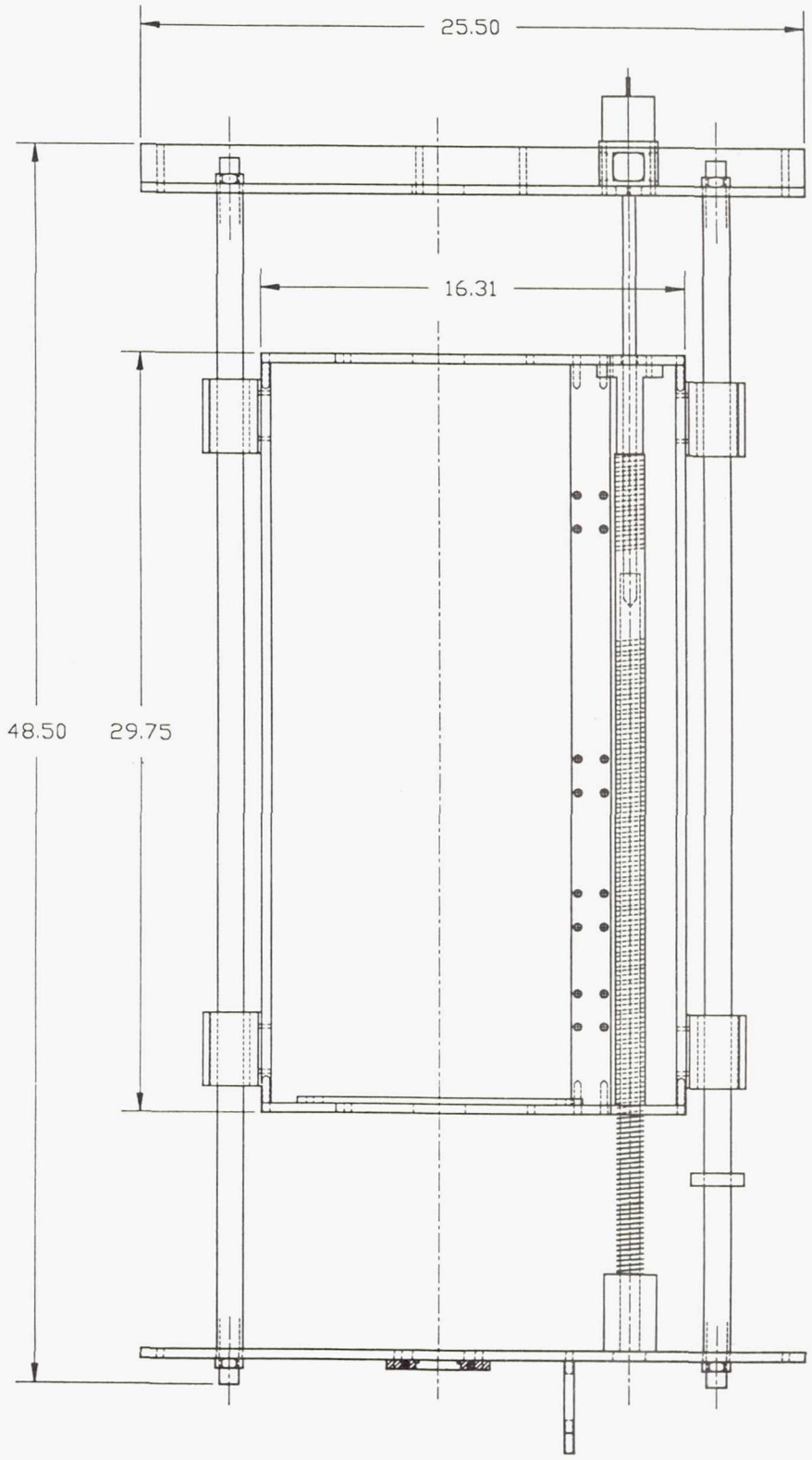

Assembly of Furnace Cage and Support Plates	
Drawing No: UAH-CMMR 0013	
Drawing Inspected By: Michael Banish	
Drawing Approved By: Dr. Franz Rosenberger	
University of Alabama in Huntsville Center for Microgravity and Materials Research	
Scale: 1.00 : 4.00	20 Jul 1989
Drawn By: Raymond R. York	
BAZ Space Company {A}	

Furnace Cage Top Plate

3/8 inch Al

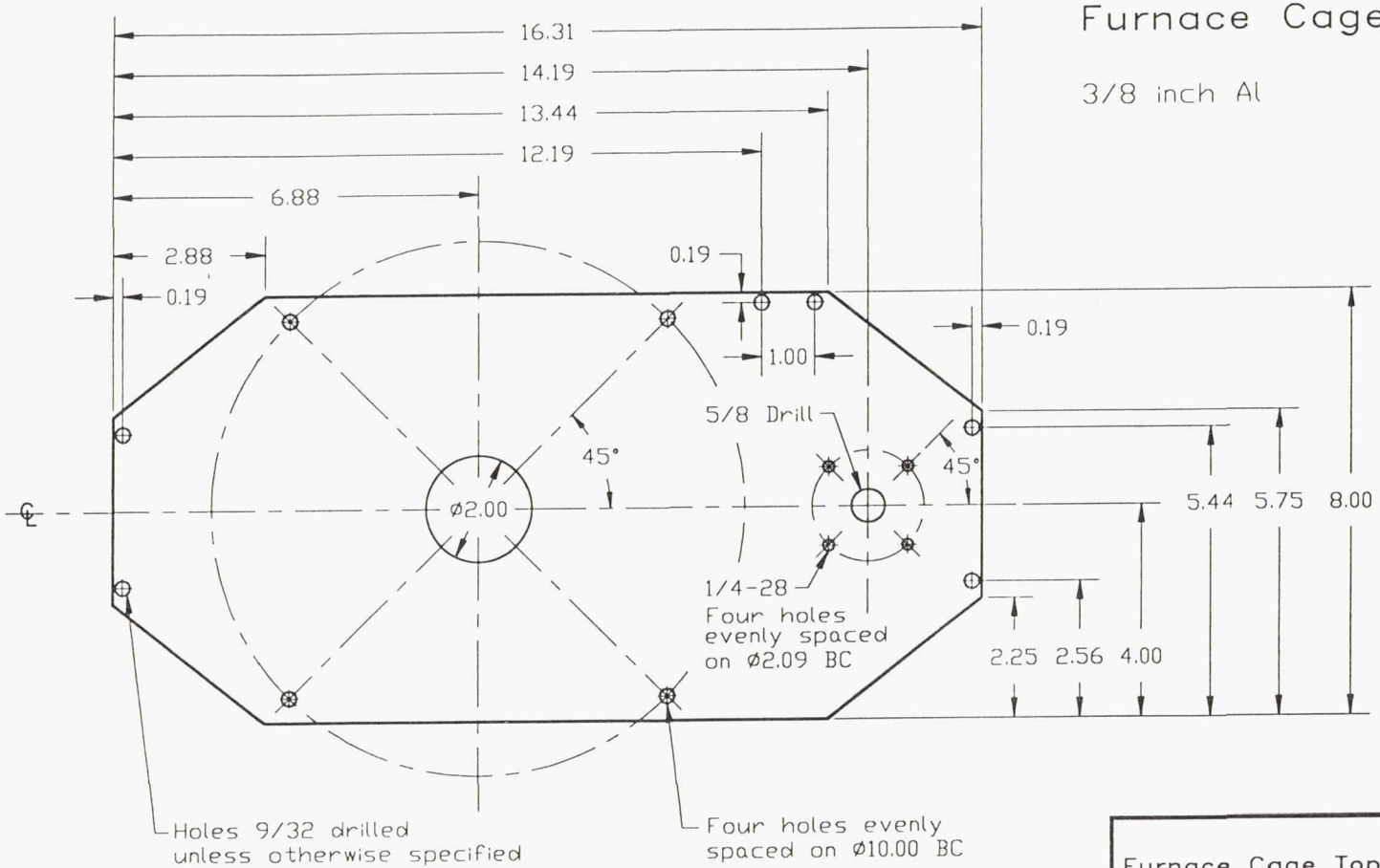

Furnace Cage Top Plate	20Jul1989
Drawing No: UAH-CMMR 0001	Scale: 1.00 : 2.00
Drawing Inspected By: Michael Banish	Drawn By: Raymond R. Yoel
Drawing Approved By: Dr. Franz Rosenberger	BAZ Space Company {B}
University of Alabama in Huntsville Center for Microgravity and Materials Research	

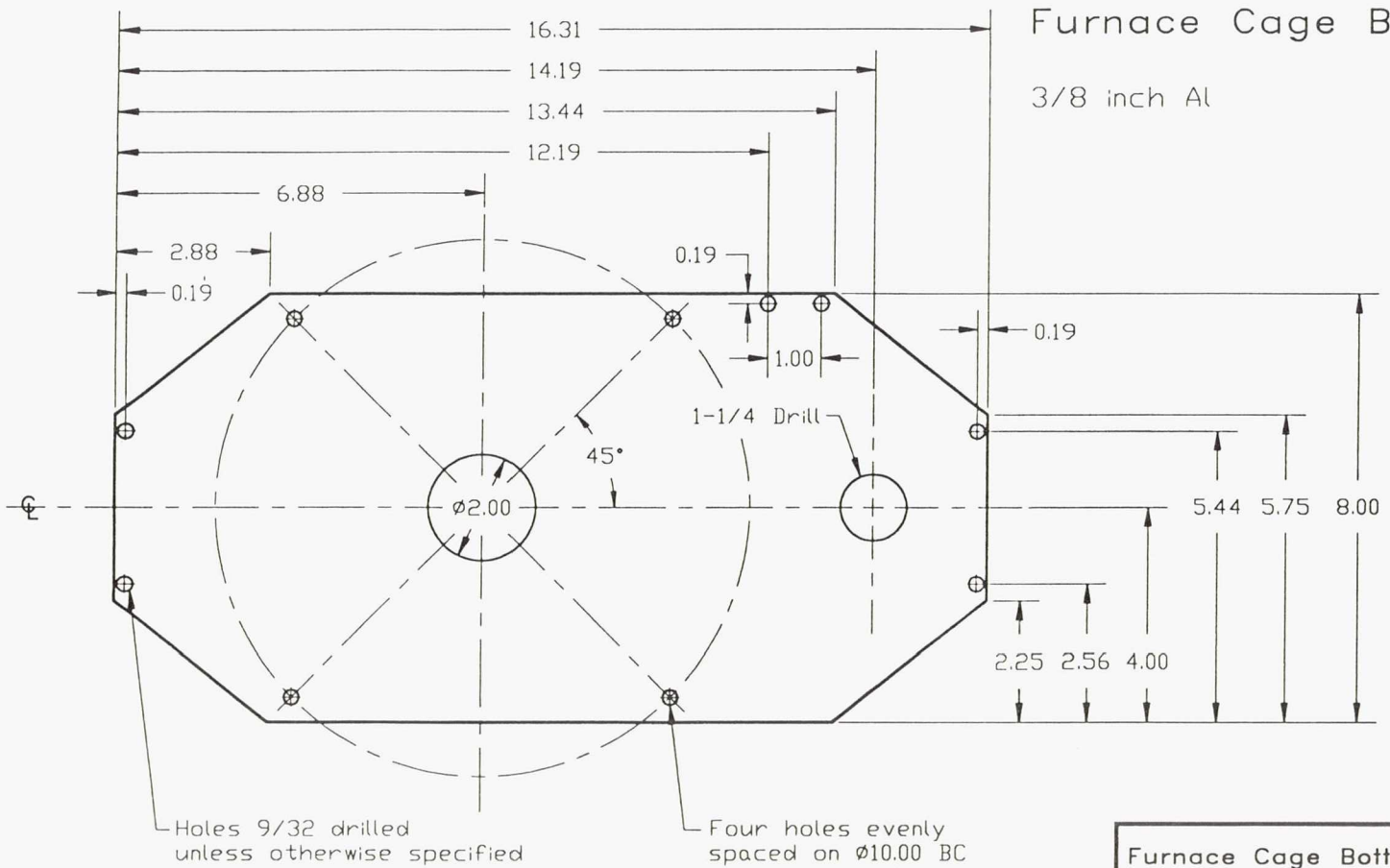

Furnace Cage Bottom Plate

3/8 inch Al

Furnace Cage Bottom Plate	20Jul1989
Drawing No: UAH-CMMR 0002	Scale: 1.00 : 2.00
Drawing Inspected By: Michael Banish	Drawn By : Raymond R. Yoel
Drawing Approved By: Dr. Franz Rosenberger	BAZ Space Company
University of Alabama in Huntsville Center for Microgravity and Materials Research	{C}

Furnace Cage Side Plate

3/8 inch Al

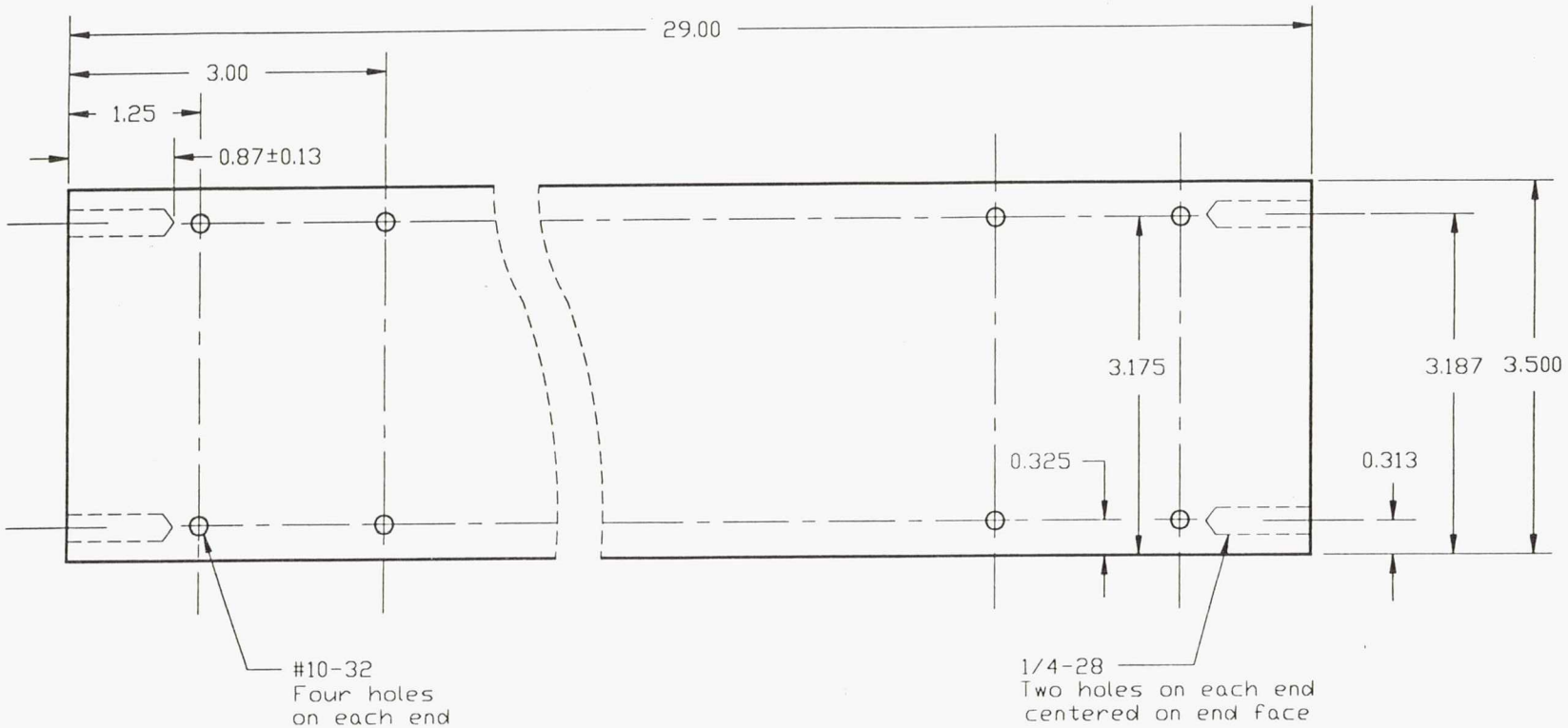

Furnace Cage Side Plate	20Jul1989
Drawing No: UAH-CMMR 0005	Scale: 1.00 : 1.00
Drawing Inspected By: Michael Banish	Drawn By : Raymond R. Yoel
Drawing Approved By: Dr. Franz Rosenberger	BAZ Space Company
University of Alabama in Huntsville Center for Microgravity and Materials Research	{D}

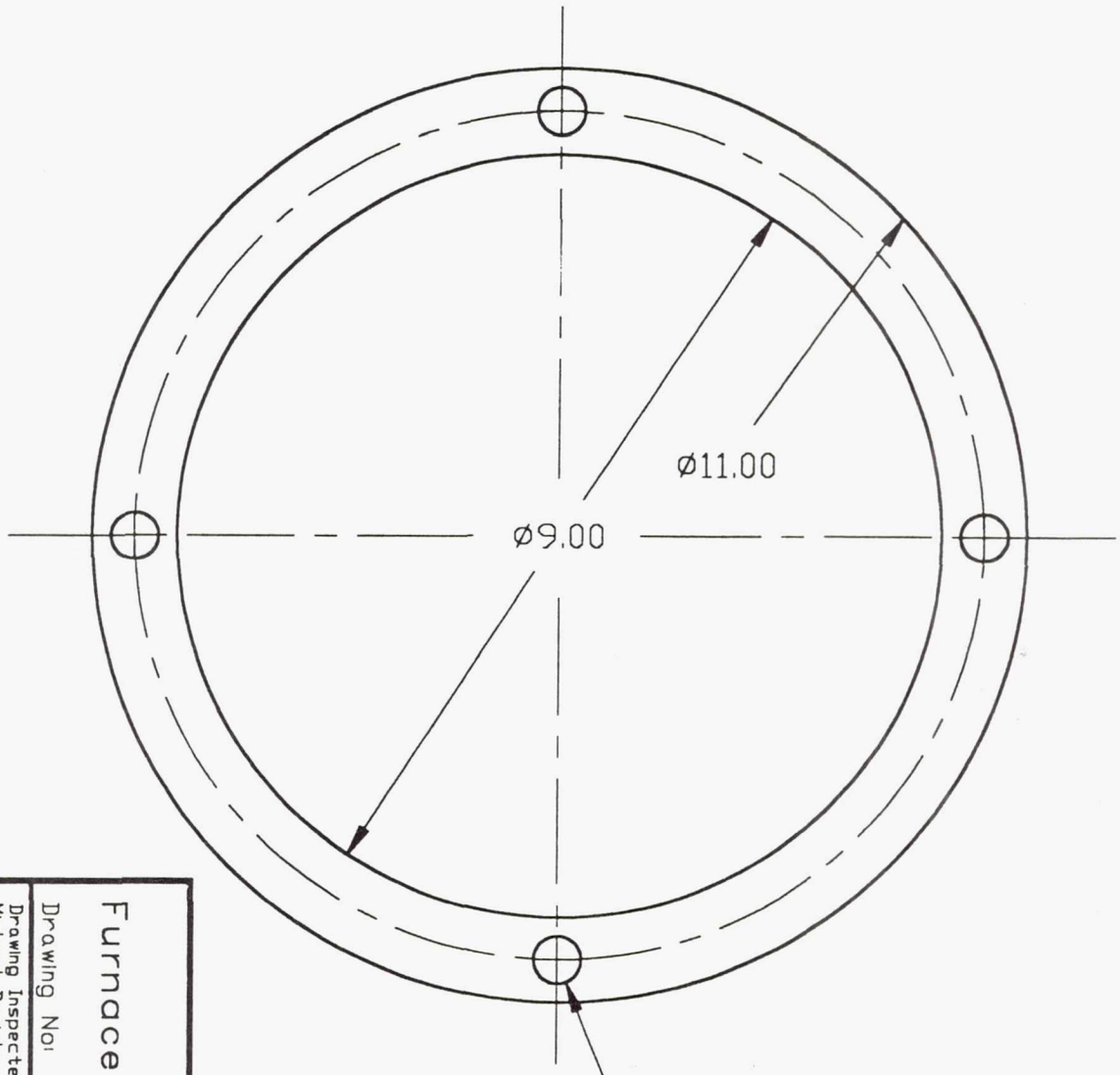

Furnace Ring Support

1/4 inch Al

Furnace Ring Support

Drawing No: UAH-CMMR 0012

Drawing Inspected By:
Michael Banish

Drawing Approved By:
Dr. Franz Rosenberger

University of Alabama in Huntsville
Center for Microgravity and
Materials Research

Drawn By :
Raymond R. Yoel

20Jul1989

Scale: 1.00 : 2.00

BAZ Space Company

{E}

Furnace Cage Back Support Plate

3/8 inch Al

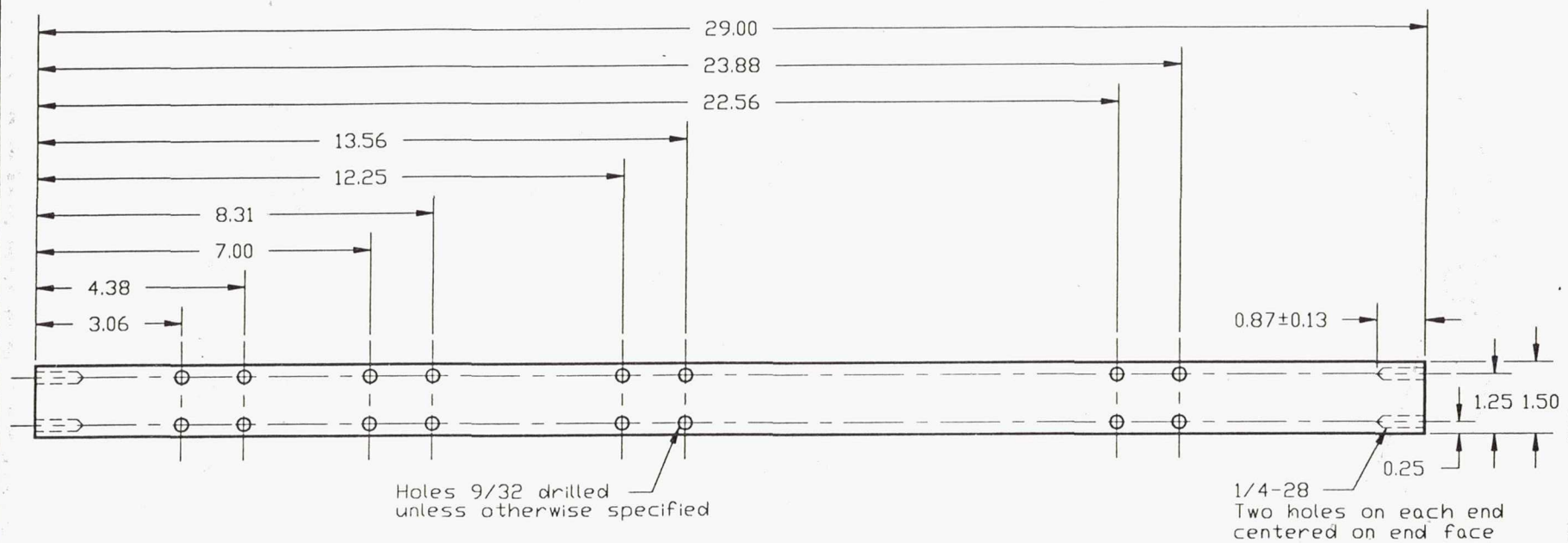

Furnace Cage Back Support Plate	20Jul1989
Drawing No: UAH-CMMR 0006	Scale: 1.00 : 2.00
Drawing Inspected By: Michael Banish	Drawn By : Raymond R. Yoel
Drawing Approved By: Dr Franz Rosenberger	BAZ Space Company {F}
University of Alabama in Huntsville Center for Microgravity and Materials Research	

Top Support Plate

3/8 inch Al

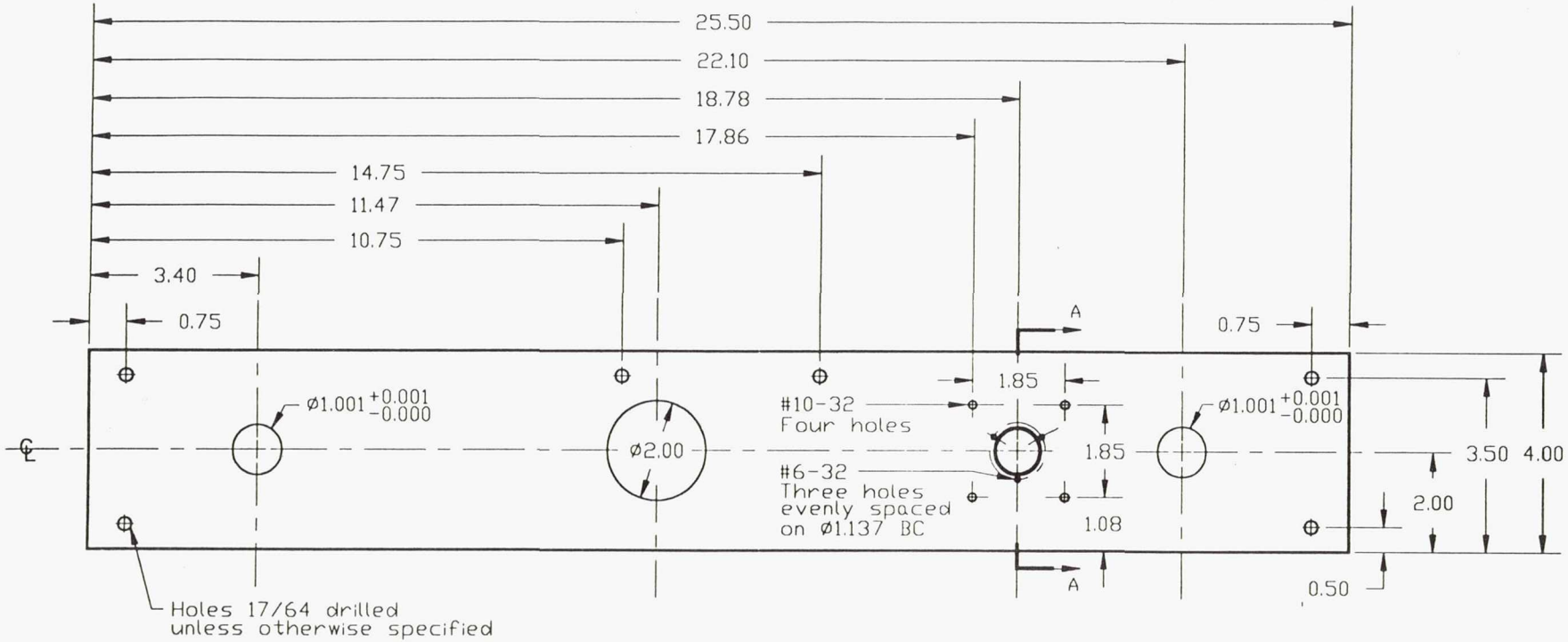

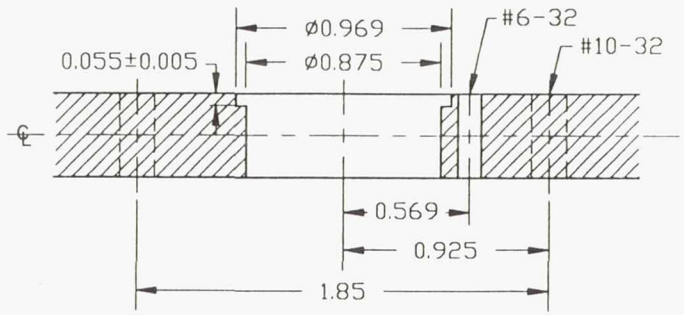

Section A-A

Scale: 2.00 : 1.00

Top Support Plate	20Jul1989
Drawing No: UAH-CMMR 0003	Scale: 1.00 : 2.00
Drawing Inspected By: Michael Banish	Drawn By : Raymond R. Yoel
Drawing Approved By: Dr. Franz Rosenberger	BAZ Space Company
University of Alabama in Huntsville Center for Microgravity and Materials Research	{G}

Top Support Bar

3/4 inch Al

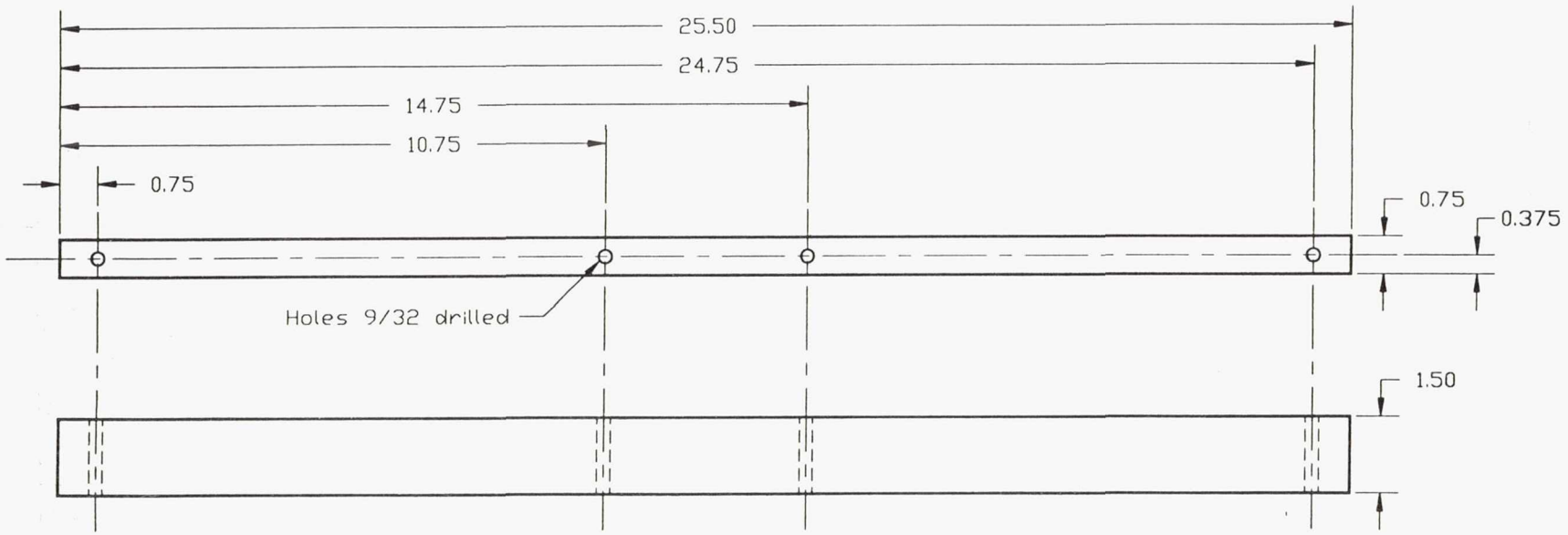

Top Support Bar	20Jul1989
Drawing No: UAH-CMMR 0011	Scale: 1.00 : 2.00
Drawing Inspected By: Michael Banish	Drawn By : Raymond R. Yoel
Drawing Approved By: Dr. Franz Rosenberger	BAZ Space Company
University of Alabama in Huntsville Center for Microgravity and Materials Research	{H}

Bottom Support Plate

3/8 inch Al

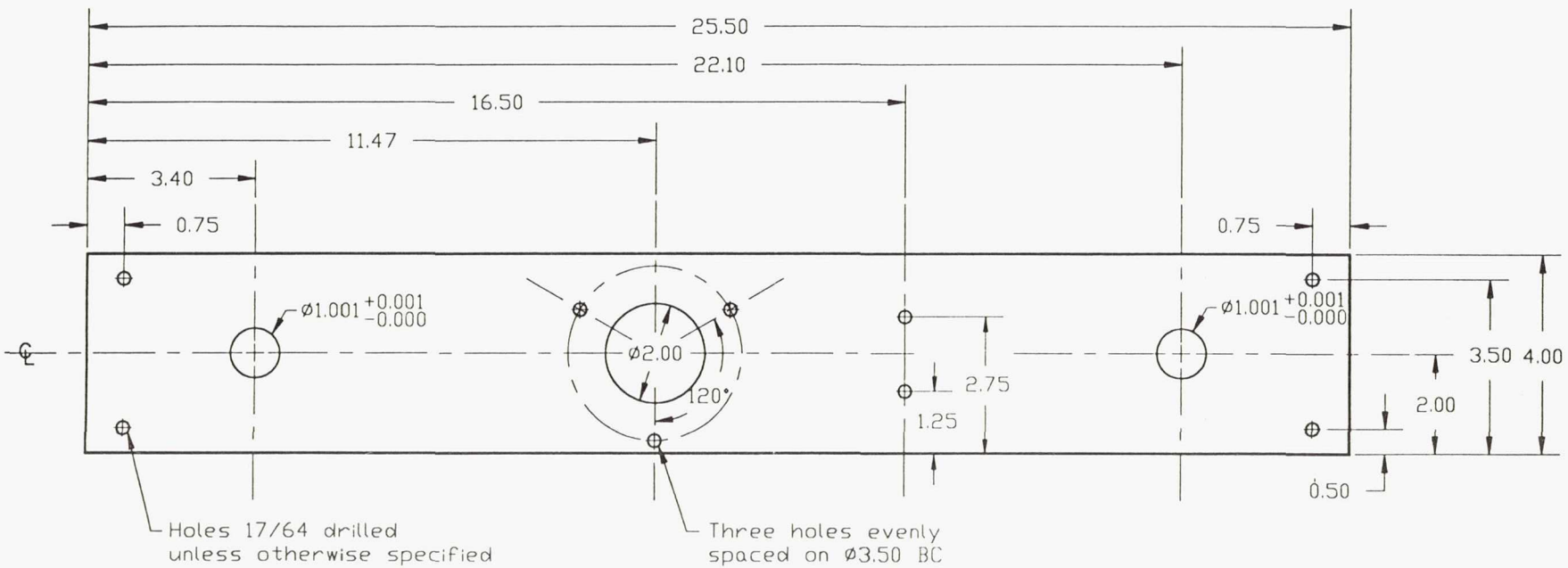

Bottom Support Plate	20Jul1989
Drawing No: UAH-CMMR 0004	Scale: 1.00 : 2.00
Drawing Inspected By: Michael Banish	Drawn By: Raymond R. Yoel
Drawing Approved By: Dr. Franz Rosenberger	BAZ Space Company
University of Alabama in Huntsville Center for Microgravity and Materials Research	{I}

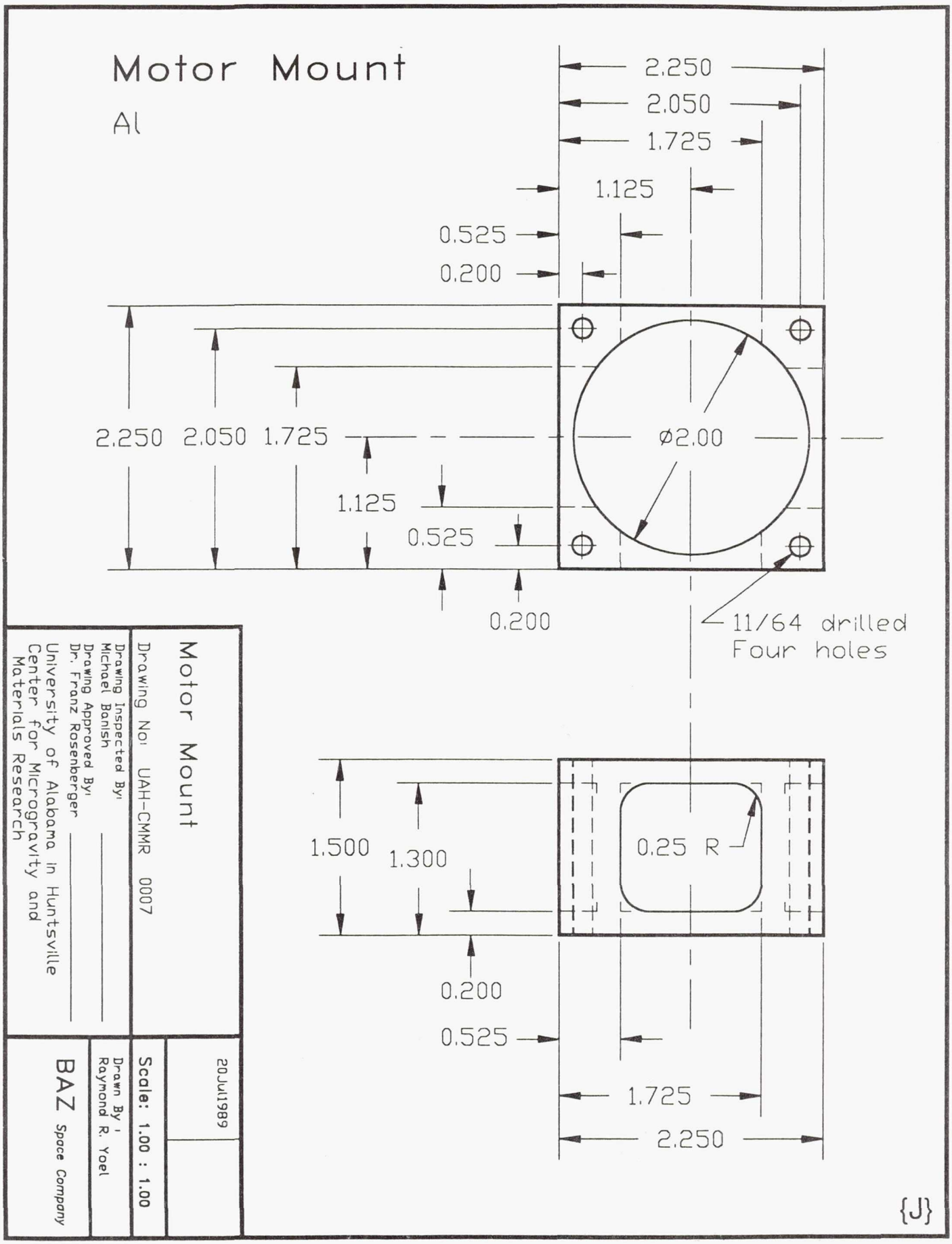
Motor Mount
Al
2.250
2.050
1.725
1.125
0.525
0.200
2.250
2.050
1.725
1.125
0.525
0.200
ø2.00
11/64 drilled
Four holes
1.500
1.300
0.25 R
0.200
0.525
1.725
2.250
{J}
Motor Mount
Drawing No: UAH-CMMR 0007
Drawing Inspected By:
Michael Banish
Drawing Approved By:
Dr. Franz Rosenberger
University of Alabama in Huntsville
Center for Microgravity and
Materials Research
20Jul1989
Scale: 1.00 : 1.00
Drawn By:
Raymond R. Yoel
BAZ Space Company

Split Collet for vacuum valve support

3/8 inch Al

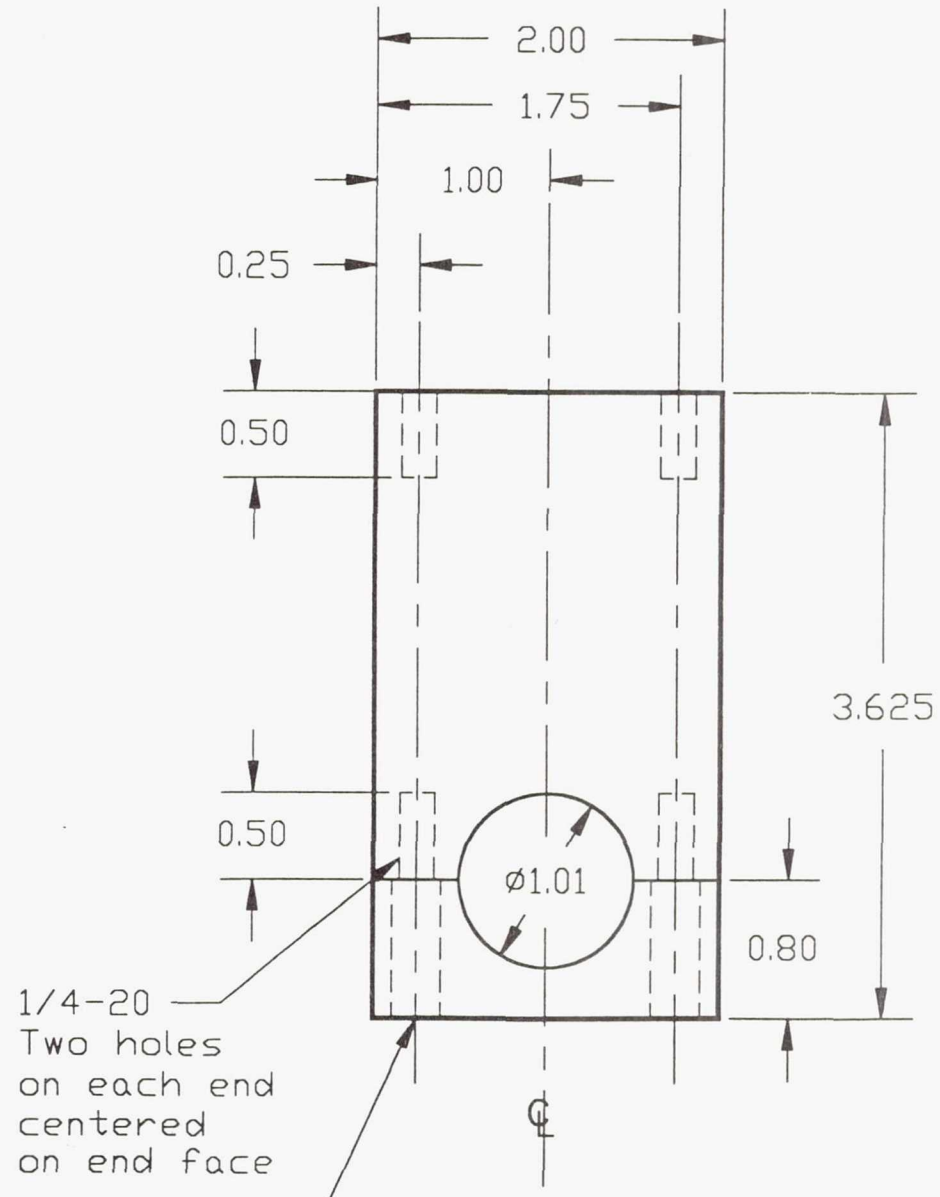

{K}

Split Collet for vacuum valve support

Drawing No: UAH-CMMR 0009

Drawing Inspected By: Michael Banish

Drawing Approved By: Dr. Franz Rosenberger

University of Alabama in Huntsville
Center for Microgravity and
Materials Research

20Jul1989

Scale: 1.00 : 1.00

Drawn By: Raymond R. Yoel

BAZ Space Company

Split Collet for vacuum port interface

3/8 inch Al

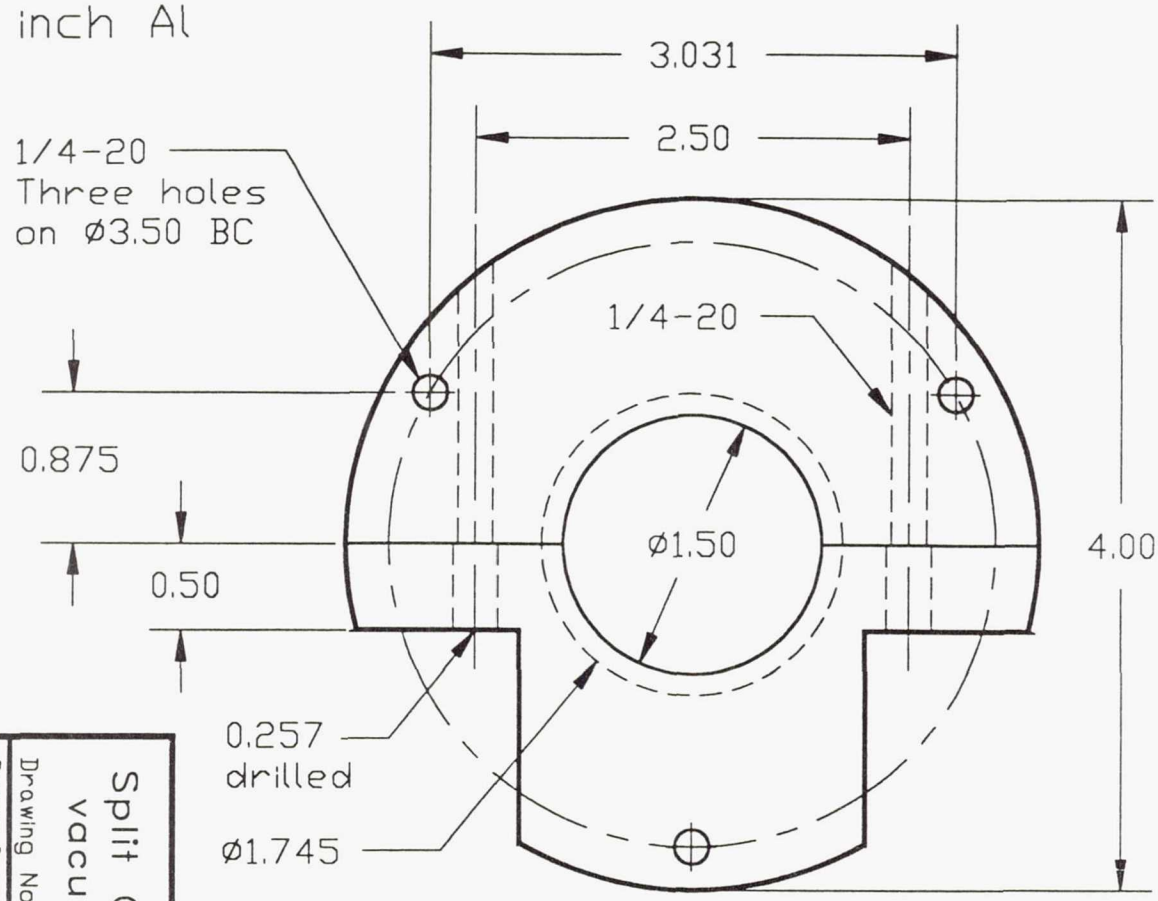

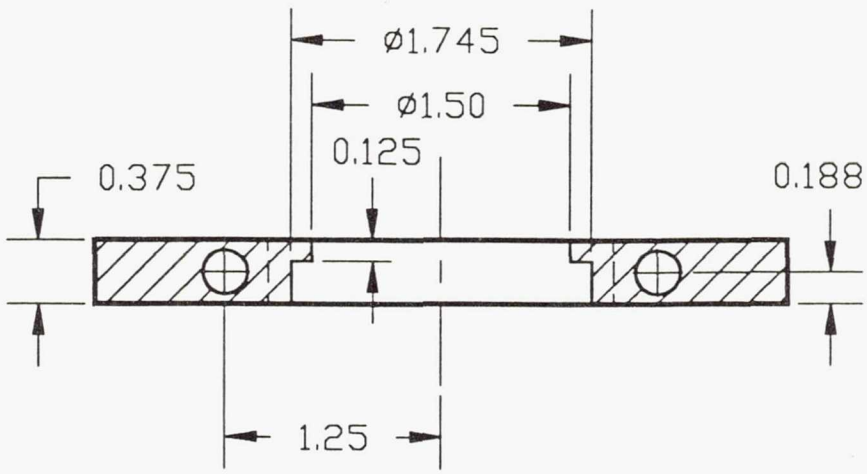

Split Collet for vacuum port interface

Drawing No: UAH-CMMR 0010

Drawing Inspected By: Michael Banish

Drawing Approved By: Dr. Franz Rosenberger

University of Alabama in Huntsville
Center for Microgravity and
Materials Research

Drawn By: Raymond R. Yoel

20Jul1989

Scale: 1.00 : 1.00

BAZ Space Company

{L}

5. REFERENCES

1. Rosenberger, F.: Fluid Dynamics in Crystal Growth from Vapors. Physico Chemical Hydrodyn., vol. 1, 1980, pp. 3-26.

2. Rosenberger, F.: Fluid Dynamic Effects in Vapor Crystal Growth Ampoules. Preparation and Characterization of Materials, J.M. Honig and C.N.R. Rao, eds., Academic Press, 1981, pp. 3-28.

3. Rosenberger, F.: Convection in Vapor Crystal Growth Ampoules. Convective Transport and Instability Phenomena, J. Zierep and H. Oertel Jr., eds., Verlag Braun, Karlsruhe, 1982, pp. 469-489.

4. Leamy, H.J.; Gilmer, G.H.; and Jackson, K.A.: Statistical Thermodynamics of Clean Surfaces. Surface Physics of Materials, J.M. Blakely, ed., Academic Press, 1975, Vol. 1, pp. 121-188.

5. Chen, J.-S.; Ming, N.-B.; and Rosenberger, F.: On the Atomic Roughness of Vapor-Solid Interfaces: Significance of Many-Body Interactions. J. Chem. Phys., vol. 84, no. 4, Feb. 15, 1986, pp. 2365-2375.

6. Chernov, A.A.: Stability of Faceted Shapes. J. Crystal Growth, vol. 24/25, 1974, pp. 11-31.

7. Rosenberger, F., et al.: Constitutional Supersaturation Revisited. J. Crystal Growth, vol. 29, 1975, pp. 49-54.

8. Narayanan, H.; Youngquist, G.R.; and Estrin, J.: Nonuniform Solution Growth of Potassium Aluminum Sulfate. J. Colloid Interface Sci., vol. 85, 1982, pp. 319-331.

9. Xiao, R.-F.; Alexander, J.I.D.; and Rosenberger, F.: Morphological Evolution of Growing Crystals: A Monte Carlo Simulation. Phys. Rev. A., vol. 38, Sept. 1, 1988, pp. 2447-2456.

10. Xiao, R.-F.; Alexander, J.I.D.; and Rosenberger, F.: Growth Morphology with Anisotropic Surface Kinetics. J. Crystal Growth, vol. 100, 1990, pp. 313-329.

11. Ostrach, S.: Fluid Mechanics in Crystal Growth - The 1982 Freeman Scholar Lecture, J. Fluids Eng., vol. 105, no. 1, Mar. 1983, pp. 5-20.

12. Greenwell, D.W.; Markham, B.L.; and Rosenberger, F.: Numerical Modeling of Diffusive Physical Vapor Transport in Cylindrical Ampoules. J. Crystal Growth, vol. 51, 1981, pp. 413-425.

13. Markham, B.L.; Greenwell, D.W.; and Rosenberger, F.: Numerical Modeling of Diffusive-Convective Physical Vapor Transport in Cylindrical Vertical Ampoules. J. Crystal Growth, vol. 51, 1981, pp. 426-437.

14. Abernathey, J.R.; Greenwell, D.W.; and Rosenberger, F.: Congruent (Diffusionless) Vapor Transport. J. Crystal Growth, vol. 47, 1979, pp. 145-154.

15. Schiroky, G.H.; and Rosenberger, F.: Free Convection of Gases in a Horizontal Cylinder with Differentially Heated End Walls. Int. J. Heat Mass Trans., vol. 27, 1984, pp. 587-598.

16. Olson, J.M.; and Rosenberger, F.: Convective Instabilities in a Closed Vertical Cylinder Heated from Below. J. Fluid Mech., vol. 92, pt. 4, June 27, 1979, pp. 609-642.

17. Abernathey, J.R.; and Rosenberger, F.: Soret Diffusion and Convective Stability in a Closed Vertical Cylinder. Phys. Fluids, vol. 24, no. 3, Mar. 1981, pp. 377-381.

18. Rosenberger, F.; and Westphal, G.H.: Low Stress Physical Vapor Growth (PVT). J. Crystal Growth, vol. 43, 1978, pp. 148-152.

19. Rosenberger, F.: Diffusionless Vapor Growth of CdS Single Crystals. Final Report Contract DAAHO1-81-C-B110 to U.S. Army MICOM, 1982. (Avail. NTIS, AD-B085931L.)

20. Feigelson, R.S., Route, R.; and Kao, T.-M.: Growth of Urea Crystals by Physical Vapor Transport. J. Crystal Growth, vol. 72, 1985, pp. 585-594.

21. Kuwamoto, H.: Seeded Growth of Large Single-Grain CdTe From the Vapor Phase. J. Crystal Growth, vol. 69, 1984, pp. 204-206.

22. Rosenberger, F.: Fundamentals of Crystal Growth I. Macroscopic Equilibrium and Transport Concepts. Springer, Berlin, 1979.

23. Sekerka, R.F.: Morphological Stability. Crystal Growth: An Introduction, P. Hartman, ed., North Holland, 1973, pp. 403-443.

24. Wollkind, D.J.: A Deterministic Continuum Mechanical Approach to Morphological Stability of the Solid-Liquid Interface. Morphological Stability, Convection, Graphite, and Integrated Optics, Preparation and Properties of Solid State Materials, Vol. 4, W.R. Wilcox, ed., Dekker, 1979, pp. 111-191.

25. Kröger, F.A.: The Chemistry of Imperfect Crystals. North-Holland, 1973.

26. Mercier, J.: Recent Developments in Chemical Vapor Transport in Closed Tubes. J. Crystal Growth, vol. 56, 1982, pp. 235-244.

27. Hirth, J.P.; and Pound, G.M.: Condensation and Evaporation. Pergamon, 1963.

28. Russell, G.J.; and Woods, J.: The Growth of CdS in Sealed Silica Capsules. J. Crystal Growth, vol. 46, 1979, pp. 323-330.

29. Reed, T.B.; LaFleur, W.J.; and Strauss, A.J.: Diffusion and Convection in Vapor Crystal Growth. J. Crystal Growth, vol. 3/4, 1968, pp. 115-121.

30. Reed, T.B.; and LaFleur, W.J.: Constitutional Supercooling in Iodine Vapor Crystal Growth. Appl. Phys. Lett., vol. 5, 1964, pp. 191-193.

31. Vohl, P.: A Technique for Vapor Phase Growth of Zinc Selenide. Mater. Res. Bull., vol. 4, 1969, pp. 689-698.

32. Markham, B.L.; and Rosenberger, F.: Diffusive-Convective Vapor Transport Across Horizontal and Inclined Rectangular Enclosures. J. Crystal Growth, vol. 67, 1984, pp. 241-254.

33. Smutek, C., et al.: Three-Dimensional Convection in Horizontal Cylinders: Numerical Solutions and Comparison with Experimental and Analytical Results. Numer. Heat Trans., vol. 8, 1985, pp. 613-631.

34. Bontoux, P., et al.: Convection in the Vertical Midplane of a Horizontal Cylinder. Comparison of Two-Dimensional Approximations with Three-Dimensional Results. Int. J. Heat Mass Trans. vol. 29, 1986, pp. 227-240.

35. Bontoux, P., et al.: Numerical Solutions and Experimental Results for Three-Dimensional Buoyancy-Driven Flows in Tilted Cylinders. Adv. Space Res., vol. 6, 1986, pp. 155-160.

36. Kaldis, E.: Principles of the Vapor Growth of Single Crystals. Crystal Growth Theory and Techniques, Vol. 1, C.H.L. Goodman, ed., Plenum, 1974, pp. 49-191.

37. Schönherr, E.: The Growth of Large Crystals from the Vapor Phase. Crystals, Growth and Properties, Vol. 2, H.C. Freyhardt, ed., Springer, 1980, pp. 51-118.

38. Faktor, M.M.; and Garrett, I.: Growth of Crystals from the Vapour. Chapman and Hall, 1974.

39. Rosenberger, F.; DeLong, M.C.; and Olson, J.M.: Heat Transfer and Temperature Oscillations in Chemical Vapor Transport Crystal Growth. J. Crystal Growth, vol. 19, 1973, pp. 317-328.

40. Tamari, N.; and Shtrikman, H.: Non-Seeded Growth of Large Single $Pb_{1-x}Sn_xTe$ Crystals on a Quartz Surface. J. Crystal Growth, vol. 43, 1978, pp. 378-380.

41. Omaly, J.; Robert, M.; and Cadoret, R.: Controle de la Croissance Cristalline, a Portir de la Phase Vapeur, en Tube Fermé, Mater. Res. Bull., vol. 16, 1981, pp. 785-792.

42. Launay, J.C.: Etude de l'influence de la convection sur la vitesse de transport par reaction chimique dans une ampoule placee dans toris zones de temperature. J. Crystal Growth, vol. 60, 1982, pp. 185-190.

43. Markov, E.V.; and Davydov, A.A.: Sublimation of CdS Crystals. Inorg. Mater. vol. 7, 1971, pp. 503-506.

44. Markov, E.V.; and Davydov, A.A.: Growing Oriented Single Crystals of Cadmium Sulfide from the Vapor Phase. Inorg. Mater., vol. 11, 1975, pp. 1504-1506.

45. Bulakh. B.M. et al.: Growth of Bulk Zinc Chalcogenide Single Crystals from the Vapor Phase and their Use for Laser Screens of Projection Colour Television. Kristall Technik, vol. 15, 1980, pp. 995-1002.

46. Golacki, Z.; et al.: Vapour Phase Growth of CdTe. J. Crystal Growth, vol. 56, 1982, pp. 213-214.

47. Golacki, Z., et al.: Vapour Phase Growth of Large Crystals of PbTe and $Pb_{1-x}Sn_xTe$. J. Crystal Growth, vol. 60, 1982, pp. 150-152.

48. Glebkin, A.A.; Davydov, A.A.; and Garba, N.I.: Growing Large Single Crystals of CdTe from the Vapor Phase. Inorg. Mater., vol. 16, 1980, pp. 19-21.

49. Klinkova, et al.: Growth of CdTe Crystals from the Vapor Phase on a Substrate out of Contact with the Capsule Walls. Inorg. Mater., vol. 19, 1983, pp. 1157-1160.

50. Davydov, A.A.; and Glebkin, A.A.: Improvements to the Process of Growing $A^{II}B^{VI}$ Crystals from the Gas Phase. Inorg. Mater., vol. 8, 1972, pp. 1523-1525.

51. Wiedemeier, H., et al.: Crystal Growth and Transport Rates of GeSe and GeTe in Micro-Gravity Environment. J. Crystal Growth, vol. 31, 1975, pp. 36-43.

52. Wiedemeier, H., et al.: Morphology and Transport Rates of Mixed IV-VI Compounds in Micro-Gravity. J. Electrochem. Soc., vol. 124, 1977, pp. 1095-1102.

53. Wiedemeier, H.: Experiments on D-1 Mission. Private communication, 1990.

54. Van den Berg, L.; and Schnepple, W.F.: Growth of Single Crystals of Mercuric Iodide (HgI_2) in Spacelab III. Materials Processing in the Reduced Gravity Environment of Space, G.E. Rindone, ed., North Holland, 1982, pp. 439-444.

55. Van den Berg, L.; and Schnepple, W.F.: Mercuric Iodide Crystal Growth in Space. Nucl. Instr. Meth. Phys. Res., vol. A283, 1989, pp. 335-338.

56. Cadoret, R.; Prisson, P.; and Fries, E.: Nucleation and Growth of HgI_2. SL-3 Science Conference, Marshall Space Flight Center, Huntsville, AL, Dec. 1985.

57. Siffert, P., et al.: Characterization of CdTe Crystals Grown Under Microgravity Conditions. Nucl. Inst. Methods Phys. Res., vol. A283, 1989, pp. 363-369.

58. Manufacturing in Space: Processing Problems and Advances. V.S. Avduyevsky, ed., MIR Publishers, Moscow, 1985.

59. Experiment Facilities for Science and Applications under Microgravity. National Space Development Agency of Japan, 1985.

60. Brebrick, R.F.; and Strauss, A.J.: Partial Pressures and Gibbs Free Energy of Formation for Congruently Subliming CdTe(c). J. Phys. Chem. Solids, vol. 25, 1964, pp. 1441-1445.

61. de Nobel, D.: Phase Equilibria and Semiconducting Properties of Cadmium Telluride. Phillips Res. Rept., vol. 14, 1959, pp. 361-399,430-492.

62. Albers, A.: Physical Chemistry of Defects. Physics and Chemistry of II-VI Compounds, M. Aven and J.S. Prener, eds., North-Holland, 1967, Chpt. 4.

63. Durose, K.; and Russell, G.J.: Twinning in CdTe. J. Crystal Growth, vol. 101, 1990, pp. 246-250.

64. Thomas, R.N., et al.: Meeting Device Needs Through Melt Growth of Large-Diameter Elemental and Compound Semiconductors. J. Crystal Growth, vol. 99, 1990, pp. 643-653.

65. Zanio, K.: Semiconductors and Semimetals, Vol. 13, Cadmium Telluride. Academic Press, 1978.

66. Brown, M.: CdTe for Infrared Detector Materials Substrates. AACG Newsletter, vol. 18, 1988, p. 3, and private communications.

67. Weast, R.C., ed.: Handbook of Chemistry and Physics, CRC Press, 1989.

68. Lange's Handbook of Chemistry, McGraw-Hill, 1988.

69. Yokota, K., et al.: Relationship Between Etch Pit Densities and Oxygen Concentrations on CdTe. Appl. Phys. Lett., vol. 56, 1990, pp. 866-867.

70. Azoulay, M., et al.: Crystalline Perfection of Melt-Grown CdTe. J. Crystal Growth, vol. 101, 1990, pp. 256-260.

71. Sen, S., et al.: Crystal Growth of Large-Area Single-Crystal CdTe and CdZnTe by the Computer-Controller Vertical Modified-Bridgman Process. J. Crystal Growth, vol. 86, 1988, pp. 111-117.

72. Song, W.-B.; Yu, M.-Y.; and Wu, W.-H.: Crystal Growth and Characterization of CdTe from the Melt under Controlled Cd Partial Pressure. J. Crystal Growth, vol. 86, 1988, pp. 127-131.

73. Lay, K.Y., et al.: High Quality, Single Crystal CdTe Grown by a Modified Horizontal Bridgman Technique. J. Crystal Growth, vol. 86, 1988, pp. 118-126.

74. Cheuvart, P., et al.: CdTe and CdZnTe Crystal Growth by Horizontal Bridgman Technique. J. Crystal Growth, vol. 101, 1990, pp. 270-274.

75. Tuller, H.L.; Uematsu, K.; and Bowen, H.K.: Vapor Growth of CdTe Laser Window Materials. J. Crystal Growth, vol. 42, 1977, pp. 150-156.

76. Igaki, K.; and Mochizuki, K.: Vapor Phase Transport of Cadmium Telluride. J. Crystal Growth, vol. 24/25, 1974, pp. 162-165.

77. Igaki, K.; Ohashi, N.; and Mochizuki, K.: Vapor Phase Transport of Cadmium Telluride, under Controlled Partial Pressure of Constituent Element. Jpn. J. Appl. Phys., vol. 15, 1976, pp. 1429-1433.

78. Mochizuki, K.: Effect of the Deviation from Stoichiometry of a Source Specimen on the Vapor Transport of CdTe. J. Crystal Growth, vol. 51, 1981, pp. 453-456.

79. Mochizuki, K.: Effect of Supersaturation on the Vapor Phase Transport of CdTe. J. Crystal Growth, vol. 53, 1981, pp. 355-360.

80. Mochizuki, K.: Vapor Growth of CdTe at Low Temperatures. J. Crystal Growth, vol. 73, 1985, pp. 510-514.

81. Geibel, C.; Maier, H.; and Schmitt, R.: Vapor Growth of CdTe as Substrate Material for $Hg_{1-x}Cd_xTe$ Epitaxy. J. Crystal Growth, vol. 86, 1988, pp. 386-390.

82. Yellin, N.; Eger, D.; and Shachna, S.: Vertical Unseeded Vapor Growth of Large CdTe Crystals. J. Crystal Growth, vol. 60, 1982, pp. 343-348.

83. Yellin, N.; and Szapiro, S.: Vapor Transport of Nonstoichiometric CdTe in Closed Ampoules. J. Crystal Growth, vol. 69, 1984, pp. 555-560.

84. Yellin, N.; Zemel, A.; and Tenne, R.: Electrical Properties of CdTe Crystals Grown by VUVG from Nonstoichiometric Charges. J. Electronic Mater., vol. 14, 1985, pp. 85-94.

85. Yellin, N.; and Szapiro, S.: Calculation of the Partial Vapor Pressures of Tellurium and Cadmium over Non-stoichiometric CdTe in the Temperature Range 750-1050 °C. J. Crystal Growth, vol. 73, 1985, pp. 77-82.

86. Nakagawa, K.; Maeda, K.; and Takeuchi, S.: Observation of Dislocations in Cadmium Telluride by Cathodoluminescence Microscopy. Appl. Phys. Lett., vol. 34, 1979, pp. 574-575.

87. Fewster, P.F., et al.: Crystallographic Polarity and Chemical Etching of $Cd_xHg_{1-x}Te$. J. Appl. Phys., vol. 52, 1981, pp. 4568-4571.

88. Brown, P.D., et al.: The Absolute Determination of CdTe Crystal Polarity. J. Crystal Growth, vol. 101, 1990, pp. 211-215.

89. Lu, Y.-C., et al.: Etch Pit Studies in CdTe Crystals. J. Vac. Sci. Technol., vol. A3, 1985, pp. 264-270.

90. Nouruzi-Khorasani, A., et al.: Surface Damage of CdTe by Mechanical Polishing Investigated by Cross-Sectional TEM. J. Crystal Growth, vol. 102, 1990, pp. 1069-1073.

91. Lauck, R.; and Müller-Vogt, G.: Vapour Transport of Impurities in Semi-Closed Ampoules. J. Crystal Growth, vol. 74, 1986, pp. 513-519 and 520-528.

92. Bird, R.B.; Stewart, W.E.; and Lightfoot, E.N.: Transport Phenomena, Wiley, 1960, p. 46.

93. Luz, P.L.: A Comparison of Cosmic SINDA, Gaski SINDA and SINDA 85. NASA MSFC Report PD22-89-08, Sept. 1989.

94. Galloway, P.N.: Thermal Analysis and Numerical Model of an Axisymmetric Vapor Crystal Growth Furnace. Master Thesis, Department of Mechanical Engineering, Univer-sity of Alabama, 1990.

NASA
National Aeronautics and Space Administration

Report Documentation Page

1. Report No.	2. Government Accession No.	3. Recipient's Catalog No.
NASA TM–103786		

4. Title and Subtitle	5. Report Date
Vapor Crystal Growth Technology Development—Application to Cadmium Telluride	December 1991
	6. Performing Organization Code E-6062

7. Author(s)	8. Performing Organization Report No.
Franz Rosenberger, Michael Banish, and Walter M.B. Duval	674–21–05
	10. Work Unit No.

9. Performing Organization Name and Address	11. Contract or Grant No.
National Aeronautics and Space Administration Lewis Research Center Cleveland, Ohio 44135–3191	
	13. Type of Report and Period Covered Technical Memorandum
12. Sponsoring Agency Name and Address National Aeronautics and Space Administration Washington, D.C. 20546–0001	14. Sponsoring Agency Code

15. Supplementary Notes

Franz Rosenberger and Michael Banish, University of Alabama in Huntsville, Center for Microgravity and Material Research, Huntsville, Alabama 35889 (work funded by NASA Contract NAS3–25361). Walter M.B. Duval, NASA Lewis Research Center. Responsible person, Walter M.B. Duval, (216) 433–5023.

16. Abstract

A novel technology for the growth of bulk crystals by physical vapor transport has been developed and applied to cadmium telluride. In particular, this technology makes use of effusive ampoules, in which part of the vapor contents escapes to a vacuum shroud through defined leaks during the growth process. This approach has the advantage over traditional sealed ampoule techniques that impurity vapors and excess (incongruent) vapor constituents are continuously removed from the vicinity of the growing crystal. Consequently, growth rates are obtained routinely at magnitudes that are rather difficult to achieve in closed ampoules. Other advantages of this **effusive ampoule physical vapor transport** (EAPVT) technique include (i) the predetermination of transport rates based on simple fluid dynamics and engineering considerations, and (ii) the growth of the crystal from close-to-congruent vapors, which largely alleviates the compositional non-uniformities resulting from buoyancy-driven convective transport. After concisely reviewing earlier work on improving transport rates, nucleation control, and minimization of crystal-wall interactions in vapor crystal growth, this report gives a detailed technical account of the largely computer controlled EAPVT experimentation developed in our laboratory. In addition, after a summary of the earlier work on the crystal growth of cadmium telluride, our own efforts to grow this material by EAPVT are described in detail. These efforts have resulted in largely single crystalline boules of 25 mm diameter and length, with dislocation (etch pit) densities as low as 2×10^3 cm^{-2}. Tellurium precipitates were essentially limited to grain and twin boundaries. Typical carrier concentrations were 8×10^{15} cm^{-3}. Optical absorption measurements showed close to theoretical transmissivities between 860nm and 32μm, indicating high purity of the material. Further measures for the improvement of the growth conditions for obtaining better crystal quality are suggested.

17. Key Words (Suggested by Author(s))	18. Distribution Statement
Vapor crystal growth Effusive ampoule Technology development	Unclassified - Unlimited Subject Category 29

19. Security Classif. (of the report)	20. Security Classif. (of this page)	21. No. of pages	22. Price*
Unclassified	Unclassified	52	A04

NASA FORM 1626 OCT 86

*For sale by the National Technical Information Service, Springfield, Virginia 22161